# Search for Lepton Flavour Violation in ep Collisions at HERA

H1 Collaboration

Abstract

A search for the lepton flavour violating processes $ep \to \mu X$ and $ep \to \tau X$ is performed with the H1 experiment at HERA. Final states with a muon or tau and a hadronic jet are searched for in a data sample corresponding to an integrated luminosity of $66.5\,\mathrm{pb}^{-1}$ for e^+p collisions and $13.7\,\mathrm{pb}^{-1}$ for e^-p collisions at a centre-of-mass energy of $319\,\mathrm{GeV}$. No evidence for lepton flavour violation is found. Limits are derived on the mass and the couplings of leptoquarks inducing lepton flavour violation in an extension of the Buchmüller-Rückl-Wyler effective model. Leptoquarks produced in ep collisions with a coupling strength of $\lambda = 0.3$ and decaying with the same coupling strength to a muon-quark pair or a tau-quark pair are excluded at 95% confidence level up to masses of $459\,\mathrm{GeV}$ and $379\,\mathrm{GeV}$, respectively.
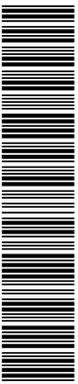
A. Aktas[10], C. Alexa[10,49], V. Andreev[24], T. Anthonis[4], B. Antunovic[25], S. Aplin[10], A. Asmone[32], A. Astvatsatourov[4], A. Babaev[23,†], S. Backovic[29], A. Baghdasaryan[37], P. Baranov[24], E. Barrelet[28], W. Bartel[10], S. Baudrand[26], M. Beckingham[10], K. Begzsuren[34], O. Behnke[13], O. Behrendt[7], A. Belousov[24], N. Berger[39], J.C. Bizot[26], M.-O. Boenig[7], V. Boudry[27], I. Bozovic-Jelisavcic[2], J. Bracinik[25], G. Brandt[13], M. Brinkmann[10], V. Brisson[26], D. Bruncko[15], F.W. Büsser[11], A. Bunyatyan[12,37], G. Buschhorn[25], L. Bystritskaya[23], A.J. Campbell[10], K.B. Cantun Avila[21], F. Cassol-Brunner[20], K. Cerny[31], V. Cerny[15,46], V. Chekelian[25], A. Cholewa[10], J.G. Contreras[21], J.A. Coughlan[5], G. Cozzika[9], J. Cvach[30], J.B. Dainton[17], K. Daum[36,42], Y. de Boer[23], B. Delcourt[26], M. Del Degan[39], A. De Roeck[10,44], E.A. De Wolf[4], C. Diaconu[20], V. Dodonov[12], A. Dubak[29,45], G. Eckerlin[10], V. Efremenko[23], S. Egli[35], R. Eichler[35], F. Eisele[13], A. Eliseev[24], E. Elsen[10], S. Essenov[23], A. Falkewicz[6], P.J.W. Faulkner[3], L. Favart[4], A. Fedotov[23], R. Felst[10], J. Feltesse[9,47], J. Ferencei[15], L. Finke[10], M. Fleischer[10], A. Fomenko[24], G. Franke[10], T. Frisson[27], E. Gabathuler[17], E. Garutti[10], J. Gayler[10], S. Ghazaryan[37], S. Ginzburgskaya[23], A. Glazov[10], I. Glushkov[38], L. Goerlich[6], M. Goettlich[10], N. Gogitidze[24], S. Gorbounov[38], M. Gouzevitch[27], C. Grab[39], T. Greenshaw[17], M. Gregori[18], B.R. Grell[10], G. Grindhammer[25], S. Habib[11,48], D. Haidt[10], M. Hansson[19], G. Heinzelmann[11], C. Helebrant[10], R.C.W. Henderson[16], H. Henschel[38], G. Herrera[22], M. Hildebrandt[35], K.H. Hiller[38], D. Hoffmann[20], R. Horisberger[35], A. Hovhannisyan[37], T. Hreus[4,43], S. Hussain[18], M. Jacquet[26], M.E. Janssen[10], X. Janssen[4], V. Jemanov[11], L. Jönsson[19], D.P. Johnson[4], A.W. Jung[14], H. Jung[10], M. Kapichine[8], J. Katzy[10], I.R. Kenyon[3], C. Kiesling[25], M. Klein[38], C. Kleinwort[10], T. Klimkovich[10], T. Kluge[10], G. Knies[10], A. Knutsson[19], V. Korbel[10], P. Kostka[38], M. Kraemer[10], K. Krastev[10], J. Kretzschmar[38], A. Kropivnitskaya[23], K. Krüger[14], M.P.J. Landon[18], W. Lange[38], G. Laštovička-Medin[29], P. Laycock[17], A. Lebedev[24], G. Leibenguth[39], V. Lendermann[14], S. Levonian[10], L. Lindfeld[40], K. Lipka[10], A. Liptaj[25], B. List[11], J. List[10], N. Loktionova[24], R. Lopez-Fernandez[22], V. Lubimov[23], A.-I. Lucaci-Timoce[10], H. Lueders[11], L. Lytkin[12], A. Makankine[8], E. Malinovski[24], P. Marage[4], Ll. Marti[10], M. Martisikova[10], H.-U. Martyn[1], S.J. Maxfield[17], A. Mehta[17], K. Meier[14], A.B. Meyer[10], H. Meyer[10], H. Meyer[36], J. Meyer[10], V. Michels[10], S. Mikocki[6], I. Milcewicz-Mika[6], D. Mladenov[33], A. Mohamed[17], F. Moreau[27], A. Morozov[8], J.V. Morris[5], M.U. Mozer[13], K. Müller[40], P. Murín[15,43], K. Nankov[33], B. Naroska[11], Th. Naumann[38], P.R. Newman[3], C. Niebuhr[10], A. Nikiforov[25], G. Nowak[6], K. Nowak[40], M. Nozicka[38], R. Oganezov[37], B. Olivier[25], J.E. Olsson[10], S. Osman[19], D. Ozerov[23], V. Palichik[8], I. Panagoulias[l,10,41], M. Pandurovic[2], Th. Papadopoulou[l,10,41], C. Pascaud[26], G.D. Patel[17], H. Peng[10], E. Perez[9], D. Perez-Astudillo[21], A. Perieanu[10], A. Petrukhin[23], I. Picuric[29], S. Piec[38], D. Pitzl[10], R. Plačakytė[10], B. Povh[12], T. Preda[10,49], P. Prideaux[17], A.J. Rahmat[17], N. Raicevic[29], T. Ravdandorj[34], P. Reimer[30], A. Rimmer[17], C. Risler[10], E. Rizvi[18], P. Robmann[40], B. Roland[4], R. Roosen[4], A. Rostovtsev[23], Z. Rurikova[10], S. Rusakov[24], F. Salvaire[10], D.P.C. Sankey[5], M. Sauter[39], E. Sauvan[20], S. Schmidt[10], S. Schmitt[10], C. Schmitz[40], L. Schoeffel[9], A. Schöning[39], H.-C. Schultz-Coulon[14], F. Sefkow[10], R.N. Shaw-West[3], I. Sheviakov[24], L.N. Shtarkov[24], T. Sloan[16], I. Smiljanic[2], P. Smirnov[24], Y. Soloviev[24], D. South[7], V. Spaskov[8], A. Specka[27], M. Steder[10], B. Stella[32], J. Stiewe[14], U. Straumann[40], D. Sunar[4], T. Sykora[4], V. Tchoulakov[8], G. Thompson[18], P.D. Thompson[3], T. Toll[10], F. Tomasz[15], D. Traynor[18], T.N. Trinh[20], P. Truöl[40], I. Tsakov[33], B. Tseepeldorj[34], G. Tsipolitis[10,41], I. Tsurin[38], J. Turnau[6], E. Tzamariudaki[25], K. Urban[14], A. Usik[24], D. Utkin[23], A. Valkárová[31], C. Vallée[20], P. Van Mechelen[4], A. Vargas Trevino[10], Y. Vazdik[24], S. Vinokurova[10], V. Volchinski[37], K. Wacker[7], G. Weber[11], R. Weber[39], D. Wegener[7], C. Werner[13], M. Wessels[10], Ch. Wissing[10], R. Wolf[13], E. Wünsch[10], S. Xella[40], W. Yan[10], V. Yeganov[37], J. Žáček[31], J. Zálešák[30], Z. Zhang[26], A. Zhelezov[23], A. Zhokin[23], Y.C. Zhu[10], J. Zimmermann[25], T. Zimmermann[39], H. Zohrabyan[37], and F. Zomer[26]

[1] *I. Physikalisches Institut der RWTH, Aachen, Germany*[a]
[2] *Vinca Institute of Nuclear Sciences, Belgrade, Serbia*
[3] *School of Physics and Astronomy, University of Birmingham, Birmingham, UK*[b]
[4] *Inter-University Institute for High Energies ULB-VUB, Brussels; Universiteit Antwerpen, Antwerpen; Belgium*[c]
[5] *Rutherford Appleton Laboratory, Chilton, Didcot, UK*[b]
[6] *Institute for Nuclear Physics, Cracow, Poland*[d]
[7] *Institut für Physik, Universität Dortmund, Dortmund, Germany*[a]
[8] *Joint Institute for Nuclear Research, Dubna, Russia*
[9] *CEA, DSM/DAPNIA, CE-Saclay, Gif-sur-Yvette, France*
[10] *DESY, Hamburg, Germany*
[11] *Institut für Experimentalphysik, Universität Hamburg, Hamburg, Germany*[a]
[12] *Max-Planck-Institut für Kernphysik, Heidelberg, Germany*
[13] *Physikalisches Institut, Universität Heidelberg, Heidelberg, Germany*[a]
[14] *Kirchhoff-Institut für Physik, Universität Heidelberg, Heidelberg, Germany*[a]
[15] *Institute of Experimental Physics, Slovak Academy of Sciences, Košice, Slovak Republic*[f]
[16] *Department of Physics, University of Lancaster, Lancaster, UK*[b]
[17] *Department of Physics, University of Liverpool, Liverpool, UK*[b]
[18] *Queen Mary and Westfield College, London, UK*[b]
[19] *Physics Department, University of Lund, Lund, Sweden*[g]
[20] *CPPM, CNRS/IN2P3 - Univ. Mediterranee, Marseille - France*
[21] *Departamento de Fisica Aplicada, CINVESTAV, Mérida, Yucatán, México*[j]
[22] *Departamento de Fisica, CINVESTAV, México*[j]
[23] *Institute for Theoretical and Experimental Physics, Moscow, Russia*[k]
[24] *Lebedev Physical Institute, Moscow, Russia*[e]
[25] *Max-Planck-Institut für Physik, München, Germany*
[26] *LAL, Université de Paris-Sud 11, IN2P3-CNRS, Orsay, France*
[27] *LLR, Ecole Polytechnique, IN2P3-CNRS, Palaiseau, France*
[28] *LPNHE, Universités Paris VI and VII, IN2P3-CNRS, Paris, France*
[29] *Faculty of Science, University of Montenegro, Podgorica, Montenegro*[e]
[30] *Institute of Physics, Academy of Sciences of the Czech Republic, Praha, Czech Republic*[h]
[31] *Faculty of Mathematics and Physics, Charles University, Praha, Czech Republic*[h]
[32] *Dipartimento di Fisica Università di Roma Tre and INFN Roma 3, Roma, Italy*
[33] *Institute for Nuclear Research and Nuclear Energy, Sofia, Bulgaria*[e]
[34] *Institute of Physics and Technology of the Mongolian Academy of Sciences , Ulaanbaatar, Mongolia*
[35] *Paul Scherrer Institut, Villigen, Switzerland*
[36] *Fachbereich C, Universität Wuppertal, Wuppertal, Germany*
[37] *Yerevan Physics Institute, Yerevan, Armenia*
[38] *DESY, Zeuthen, Germany*
[39] *Institut für Teilchenphysik, ETH, Zürich, Switzerland*[i]
[40] *Physik-Institut der Universität Zürich, Zürich, Switzerland*[i]

[41] *Also at Physics Department, National Technical University, Zografou Campus, GR-15773 Athens, Greece*

1   Introduction

In the Standard Model (SM) the particle interactions conserve lepton flavour, although there is no underlying symmetry supporting this feature. However, experimental evidence for lepton flavour violation (LFV) in solar and atmospheric neutrino oscillations has been reported [1, 2]. The experimental upper bounds on neutrino masses imply very small LFV effects in the charged lepton sector. The observation of such effects would clearly indicate new phenomena beyond the SM.

In ep collisions at HERA, LFV processes $ep \rightarrow \mu X$ or $ep \rightarrow \tau X$ lead to final states with a muon or a tau and a hadronic system X. The LFV process can proceed via the exchange of a leptoquark (LQ), a boson with both lepton and baryon quantum number which appears naturally as a colour triplet scalar or vector boson in many extensions of the SM such as grand unified theories [3], supersymmetry [4], compositeness [5] and technicolor [6].

In this paper a search for LFV phenomena is performed in ep collision data recorded during the years 1998-2000 by the H1 experiment, corresponding to an integrated luminosity of $66.5\,\mathrm{pb^{-1}}$ for e^+p collisions and $13.7\,\mathrm{pb^{-1}}$ for e^-p collisions at a centre-of-mass energy $\sqrt{s} = 319\,\mathrm{GeV}$. The present results supercede those derived in previous searches at the H1 experiment using e^+p collisions at $\sqrt{s} = 300\,\mathrm{GeV}$ [7].

2   Experimental conditions

A detailed description of the H1 detector can be found in [8]. In the following, only the detector components relevant for this analysis are briefly discussed. The origin of the H1 coordinate system is the nominal ep interaction point, with the direction of the proton beam defining the positive z-axis (forward direction). Transverse momenta and azimuthal angles are measured in the xy plane. The pseudorapidity is related to the polar angle θ by $\eta = -\ln\tan(\theta/2)$.

A tracking system consisting of central and forward detectors is used to measure charged particle trajectories and to determine the interaction vertex. The central tracker is composed of two concentric cylindrical drift chambers providing full acceptance for particles in the range $22° < \theta < 160°$, complemented by a silicon vertex detector [9] covering the range $30° < \theta < 150°$. Transverse momenta (P_T) are determined in the central region from the curvature of the particle trajectories in a magnetic field of $1.15\,\mathrm{T}$ with an effective resolution of $\sigma(P_T)/P_T \simeq 0.01 \cdot P_T(\mathrm{GeV})$. The tracking is complemented in the forward region $7° < \theta < 25°$ by a system of drift chambers perpendicular to the beam axis.

With a polar coverage of $4° < \theta < 154°$ and full azimuthal acceptance, the liquid Argon (LAr) calorimeter encloses the tracking chambers. It consists of an inner electromagnetic part with a fine granularity and an outer hadronic part with a coarser granularity. The energy resolution of the LAr calorimeter for electrons and hadrons was determined in test beam measurements to be $\sigma/E = 12\%/\sqrt{E(\mathrm{GeV})} \oplus 1\%$ and $\sigma/E = 50\%/\sqrt{E(\mathrm{GeV})} \oplus 2\%$, respectively [10]. In the backward region $153° < \theta < 178°$, the LAr calorimeter is complemented by a lead-scintillating fibre spaghetti calorimeter.

4

The iron return yoke of the magnet is instrumented with streamer tubes to identify muon tracks. Further chambers of the central muon system are positioned around the yoke to provide a precise muon track measurement in the polar range $5° < \theta < 175°$. Additional drift chambers positioned at either side of a toroidal magnet are employed to detect muons in the forward direction ($3° < \theta < 17°$).

The luminosity is determined from the rate of the Bethe-Heitler process $ep \to ep\gamma$, measured using a photon detector located close to the beam pipe at $z = -103$ m.

Electrons are identified as compact and isolated electromagnetic clusters in the calorimeter. Within the acceptance of the tracking detectors, an associated track is required. A muon candidate is identified by associating an isolated track in the forward muon system or in the inner tracking system with a track segment or an energy deposit in the instrumented iron. The hadronic final state is reconstructed from the deposits in the LAr calorimeter in combination with tracking information. The hadrons are then combined into jets using the inclusive k_T-algorithm [11] with a P_T-weighted recombination scheme where jets are treated as massless and the separation parameter is set to one.

3 LFV phenomenology and SM background processes

The LFV processes $ep \to \mu X$ and $ep \to \tau X$ can be attributed to LQs produced at HERA predominantly by electron-quark fusion.

In the framework of the Buchmüller-Rückl-Wyler (BRW) effective model [12], LQs are classified into 14 types with respect to the quantum numbers spin, isospin and chirality. Leptoquarks carry both lepton (L) and baryon (B) quantum numbers. The fermion number $F = L + 3B$ is assumed to be conserved, taking values of $F = 2$ for $e^- q$ processes and $F = 0$ for $e^+ q$ processes. Leptoquark processes proceed via s channel resonant LQ production or u channel virtual LQ exchange, as shown in figure 1. For LQ masses m_{LQ} well below the $e^\pm p$ centre-of-mass energy, the s channel production of $F = 2$ ($F = 0$) LQs in $e^- p$ ($e^+ p$) collisions dominates. For LQ masses above 319 GeV the s and u channel processes become of equal importance and both $e^- p$ and $e^+ p$ collisions have similar sensitivity to virtual effects from $F = 2$ LQs as well as from $F = 0$ LQs.

The BRW model assumes lepton flavour conservation (LFC) such that the LQs produced in ep collisions decay only to eX or $\nu_e X$ final states. These LQs are referred to in the following as first generation LQs and have been studied in a recent H1 publication [13]. A general extension of the BRW model allows for the decay of LQs to final states containing a lepton of a different flavour, i.e. μ or τ, and a jet, as illustrated in figure 1. Non-zero couplings λ_{eq_i} to an electron-quark pair and $\lambda_{\mu q_j}$ ($\lambda_{\tau q_j}$) to a muon(tau)-quark pair are assumed. The indices[1] i and j represent quark generation indices, such that λ_{eq_i} denotes the coupling of an electron to a quark of generation i, and $\lambda_{\ell q_j}$ is the coupling of the outgoing lepton ℓ to a quark of generation j.

---

[1]In the following the quark generation indices are attached only when it is relevant.

5
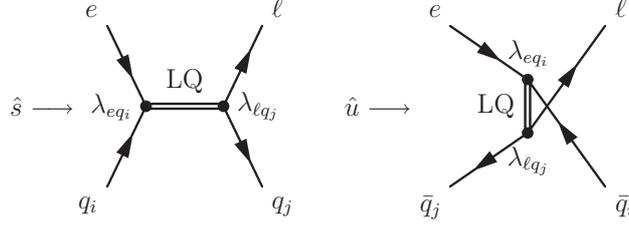
Figure 1: Left: s-channel resonant LQ production and decay to a lepton-quark pair. Right: u-channel exchange of a LQ. The indices i and j represent quark generation indices, such that λ_{eq_i} denotes the coupling of an electron to a quark of generation i, and $\lambda_{\ell q_j}$ is the coupling of the outgoing lepton ℓ to a quark of generation j. For $\ell = \mu, \tau$, the LQ introduces LFV.

The double differential cross section for the s-channel tree level process is [12]:

$$\frac{d^2\sigma_{\mathrm{s}}}{dxdy} = \underbrace{\frac{1}{32\pi\hat{s}}}_{\text{phase space}} \cdot \underbrace{\frac{\lambda_{eq}^2\lambda_{\ell q}^2\hat{s}^2}{(\hat{s}^2 - m_{\mathrm{LQ}}^2)^2 + m_{\mathrm{LQ}}^2\Gamma_{\mathrm{LQ}}^2}}_{\text{Breit-Wigner LQ propagator term}} \cdot \underbrace{q_i(x, \hat{s})}_{\text{parton density}} \times \begin{cases} \frac{1}{2} & \text{scalar LQ} \\ 2(1-y)^2 & \text{vector LQ} \end{cases} \tag{1}$$

where x is the Bjørken scaling variable, y denotes the inelasticity of the ep scattering process, $\hat{s} = sx$ represents the square of the eq centre-of-mass energy and Γ_{LQ} is the total LQ width. A similar expression holds for the u channel exchange [12].

An overview of the extended effective model for the LQ coupling to u and d quarks is given in table 1. For convenience only one LFV transition is considered: either between the first and the second generations or between the first and the third generations. The branching ratio $LQ \rightarrow \mu(\tau)q$ is given by

$$\mathrm{BR} = \beta_\ell \times \beta_{LFV} \quad \text{with} \quad \beta_{LFV} = \frac{\Gamma_{\mu(\tau)q}}{\Gamma_{\mu(\tau)q} + \Gamma_e} \quad \text{and} \quad \Gamma_{\ell q} = m_{\mathrm{LQ}}\lambda_{\ell q}^2 \times \begin{cases} \frac{1}{16\pi} & \text{scalar LQ} \\ \frac{1}{24\pi} & \text{vector LQ} \end{cases} \tag{2}$$

where $\Gamma_{\ell q}$ denotes the partial LQ decay width to a lepton $\ell = e, \mu, \tau$ and a quark q and where $\beta_\ell = \Gamma_{\ell q}/(\Gamma_{\ell q} + \Gamma_{\nu_\ell q})$ is the fraction of decays into charged leptons. Some LQs, namely S_0^L, S_1^L, V_0^L and V_1^L, can decay to a neutrino-quark pair resulting in $\beta_\ell = 0.5$. Since neutrino flavours cannot be distinguished with the H1 experiment, such final states are not covered in this search, but they are implicitly included in the search for first generation LQs [13].

To determine the signal detection efficiencies, events with LQs are generated using the LEGO [14] event generator with the CTEQ5L parametrisation of the parton distribution functions (PDF) of the proton [15]. The LQ signal expectation is a function of the LQ type, mass, coupling constant and β_{LFV}. The analysis usually requires a large number of simulated signal Monte Carlo (MC) samples. To overcome this technical difficulty, the LEGO program is used to produce a high statistics MC signal event sample generated according to a double-differential cross section $d^2\sigma_{\mathrm{generic}}/(dx\, dQ^2)$ obtained from (1) by replacing the Breit-Wigner LQ propagator term with a constant. This unique MC sample is used to calculate the efficiency to select a

LQ of a given type, mass m_{LQ}, coupling λ_{eq} and β_{LFV} by attributing to each event a weight:

$$w(\mathrm{type}, m_{\mathrm{LQ}}, \lambda_{eq}, \beta_{\mathrm{LFV}}, x, Q^2) = \frac{\frac{d^2\sigma_{\mathrm{exact}}}{dxdQ^2}(\mathrm{type}, m_{\mathrm{LQ}}, \lambda_{eq}, \beta_{\mathrm{LFV}}, x, Q^2)}{\frac{d^2\sigma_{\mathrm{generic}}}{dxdQ^2}(x, Q^2)} , \qquad (3)$$

where $Q^2 = sxy$ refers to the generated negative momentum transfer squared and x is the Bjørken scaling variable known at the generator level. This procedure provides an exact prediction over the full range of LQ production parameters and avoids approaches like the narrow width approximation or the high mass (contact interaction) approximation.

The LQ kinematics are reconstructed using the double angle method [16]. The direction of the detected lepton and jet are used to reconstruct the Bjørken scaling variable x and therefore the LQ mass $m_{\mathrm{LQ}}^{\mathrm{rec}} = \sqrt{xs}$.

The contributions from Standard Model (SM) background processes which may mimic the signal include neutral current (NC) and charged current (CC) deep-inelastic scattering (DIS), photoproduction, lepton pair production and real W boson production. These processes are briefly described below:

- **NC DIS ($ep \rightarrow eX$)**
  NC DIS processes contribute to the selected event sample if the scattered electron is attributed to the tau electronic decay or if it is misidentified as a narrow jet corresponding to a tau decay to hadrons. The NC DIS background is modelled using the event generator RAPGAP [17]. The proton PDFs are parametrised using CTEQ5L [15] and hadronisation is performed using JETSET [18] parton showers and the Lund string fragmentation.

- **CC DIS ($ep \rightarrow \nu X$)**
  Lepton flavour violating processes usually exhibit an imbalance in the measured calorimetric transverse momentum due to either the presence of a minimally ionising muon in μX final states or the escaping neutrino(s) from tau decays in τX events. This imbalance is exploited in the event selection. The CC DIS process leads to events with genuine missing transverse momentum and therefore contributes to the selected sample if hadrons or photons from the final state are misidentified as muons or if tau decays are falsely reconstructed. The CC DIS contribution is modelled using the DJANGO event generator [19].

- **Photoproduction ($\gamma p \rightarrow X$)**
  Events from photoproduction processes may contribute to the final selection if a hadron is wrongly identified as a muon or if a narrow hadronic jet fakes the tau signature. This contribution is calculated using the event generator PYTHIA [20]. CTEQ5L [15] serves as the proton PDF parametrisation and the photonic parton distribution parametrisation GRV-LO [21] is used. As PYTHIA only contains leading order $2 \rightarrow 2$ processes, the multi-jet production cross section is underestimated [22]. Therefore, the prediction is scaled up by a factor 1.2 in this analysis, in agreement with previous analyses of jets in photoproduction [22].

- **Lepton-pair production ($ep \to e\ell^+\ell^- X$)**
  Lepton-pair production events contribute to the background because they may lead to high momentum leptons in the final state. In particular, inelastic di-muon events with one unidentified muon may fake the μX LFV signature. The background samples include ee, $\mu\mu$ and $\tau\tau$ production generated with the event generator GRAPE [23].

- **W production ($ep \to eWX$)**
  Real W boson production leads to final states with isolated high P_T leptons and missing transverse momentum. The simulated W production samples are created with the event generator EPVEC [24] and include leptonic ($e\bar{\nu}_e$, $\mu\bar{\nu}_\mu$, $\tau\bar{\nu}_\tau$) and hadronic W decays.

All signal and SM samples are passed through a detailed simulation of the H1 detector response based on the GEANT program [25] and the same reconstruction and analysis algorithms as used for the data.

4 High P_T Muon Signatures

Leptoquarks with couplings to the first and the second lepton generation can be produced in ep collisions and may decay to a muon and a quark. The signature is an isolated high P_T muon back-to-back to the hadronic system in the transverse plane. In general, a muon deposits a very small fraction of its energy in the LAr calorimeter. The signal is therefore expected to exhibit large P_T^{calo}, which is the net transverse momentum reconstructed from all clusters recorded in the LAr calorimeter alone.

The event preselection requires at least one muon with a transverse momentum above $10\,\mathrm{GeV}$ in the polar angular range $10°$ to $140°$ and at least one jet. The muon is required to be isolated. The angular distance, $D = \sqrt{(\Delta\eta)^2 + (\Delta\phi)^2}$, of the muon to the nearest track and to the nearest jet is required to be greater than 0.5 and 1.0, respectively. Only events with P_T^{calo} greater than $12\,\mathrm{GeV}$ are selected. In order to further exploit the event topology in the transverse plane, the cut $V_{ap}/V_p < 0.3$ is employed, where V_{ap}/V_p is defined as the ratio of the anti-parallel to parallel projections of all energy deposits in the calorimeter with respect to the direction of P_T^{calo} [26].

Figure 2 displays the distributions of the transverse momentum of the muon, its polar angle θ_μ, P_T^{calo} and the acoplanarity $\Delta\phi_{\mu-X}$ between the muon and the hadronic final state X after the muon preselection. The data passing the preselection are well described by the SM prediction. The signal corresponding to a scalar LQ with $m_{\mathrm{LQ}} = 200\,\mathrm{GeV}$ is also shown. It displays muons with large P_T^μ produced predominantly in the forward direction (low θ_μ) in events with significant P_T^{calo} and back-to-back topology $\Delta\phi_{\mu-X} \simeq 180°$.

In the final LFV selection step, the NC DIS background is further suppressed by rejecting events with identified electrons, and by accepting only events with an imbalance of the calorimeter deposits, $P_T^{\mathrm{calo}} > 25\,\mathrm{GeV}$, and with a back-to-back topology, $\Delta\phi_{\mu-X} > 170°$. The latter selection criterion is only applied for events for which the hadronic final state is well contained in the detector, with the reconstructed polar angle $7° < \theta_X < 140°$.

The selection efficiency ranges from 40% to 60% depending on the LQ mass and type (see table 2).

8

5 High P_T Tau Signatures

Leptoquarks with couplings to the first and the third lepton generation can be produced in ep collisions and may decay to a tau and a quark. Tau leptons are identified using the electronic, muonic and hadronic decays of the tau.

5.1 Electronic tau decays

The final state resulting from the electronic tau decay, $\tau \to e\nu_e\nu_\tau$, leads to an event topology that is very similar to that of high Q^2 NC DIS events. The preselection follows that presented in [27]. A reconstructed jet with a minimal transverse momentum of $P_T^j > 25\,\text{GeV}$ back-to-back in the transverse plane to an electron with $P_T^e > 10\,\text{GeV}$ is required. The kinematic domain is restricted to $Q^2 > 1000\,\text{GeV}^2$ and $y > 0.1$. Figure 3(a) shows the distribution of P_T^{miss} after this preselection, where P_T^{miss} is defined as the total missing transverse momentum reconstructed from all observed particles.

In the final selection a large missing transverse momentum $P_T^{\text{miss}} > 20\,\text{GeV}$ is required in order to account for the expected missing momentum carried by the neutrinos produced in the tau decay. These neutrinos are boosted along the electron direction, implying an imbalance between the transverse momenta of the electron P_T^e and the hadronic final state P_T^X. Hence, the restriction $P_T^e/P_T^X < 0.8$ further reduces NC DIS background. In addition, the azimuthal distance between the missing transverse momentum and the electron must not exceed $20°$. The remaining NC DIS background, due to mismeasured electron energies leading to missing energy near the electron, is reduced by the requirement $P_T^{\text{e-clu}}/P_T^{\text{e-trk}} > 0.7$, where $P_T^{\text{e-clu}}$ is measured from the electromagnetic cluster and $P_T^{\text{e-trk}}$ from tracking information. Any events with additional isolated muons are excluded from the electronic tau decay channel. The final selection in the electronic tau decay channel yields an efficiency normalised to all tau decays of 3% to 10%, which is limited by the branching fraction $BR(\tau \to e\nu_e\nu_\tau) = 17.8\%$ [28] and dependent on the assumed LQ mass and type (see table 2).

5.2 Muonic tau decays

Muonic tau decays $\tau \to \mu\nu_\mu\nu_\tau$ result in similar final states as the high P_T muon signatures described in section 4. The same selection cuts described therein are applied here. To account for possible effects due to different muon kinematics resulting from a tau decay, the selection efficiency was studied in detail with a LFV MC signal sample with a τX final state and a subsequent muonic tau decay. The selection efficiency ranges between 4% and 8%, which is dependent on the LQ mass and type, normalised to all tau decays and limited by $BR(\tau \to \mu\nu_\mu\nu_\tau) = 17.4\%$ [28] (see table 2).

5.3 Hadronic tau decays

The hadronic decays of the high P_T tau lead to a typical signature of a high P_T "pencil-like" jet. The signal topology is a di-jet event with no leptons. The tau-jet is characterised by a narrow

energy deposit in the calorimeter and low track multiplicity with predominantly one or three tracks in the identification cone of the jet. The neutrino from the tau decay are boosted along the direction of the hadrons. The missing transverse momentum in the event is aligned with the tau-jet.

Tau-jet candidates are defined as jets with exactly one or three tracks in the tau-jet cone with an opening angle that varies between $5°$ and $30°$ with decreasing jet momentum. The tracks are required not to be associated with identified electrons or muons and the scalar sum of their transverse momenta is required to be larger than 2 GeV. The fine granularity of the LAr calorimeter is used to match extrapolated tracks with energy deposits in the calorimeter and to separate additional neutral particles associated to the tau candidate from unmatched energy deposits in the tau-jet cone. The sum of the four-vectors of the tracks and of the neutral particles defines the tau-jet candidate four-vector.

In the preselection step at least two jets with a transverse momentum $P_T^{\mathrm{jet1}} > 20\,\mathrm{GeV}$ and $P_T^{\mathrm{jet2}} > 15\,\mathrm{GeV}$ reconstructed in the polar angle range $7° < \theta_{\mathrm{jets}} < 145°$ are required. One jet must fulfil the criteria of a tau-jet candidate with $\theta_{\tau\mathrm{jet}} > 20°$. In addition, the calorimetric shower shape and tracking signature are exploited to validate the tau-jet candidates. The following estimators are used to separate a tau-jet from quark or gluon induced jets: the number of all tracks associated to the tau-jet candidate, the distance in $\eta - \phi$ between tracks and calorimetric clusters, the number of calorimeter cells of the tau-jet n_{cells}, the radial extension of the calorimetric deposits $\langle r \rangle = \sum_{i=1}^{n_{\mathrm{cells}}} E_i r_i / \sum_i E_i$, the standard deviation $\sigma(r) = \sqrt{\langle r^2 \rangle - \langle r \rangle^2}$ and the invariant tau-jet mass reconstructed from calorimeter cells. A neural net algorithm is employed and trained using the six estimator variables, as explained in [29]. The neural net yields a discriminator variable $\mathcal{D}_{NN}$ in the range $0 \leq \mathcal{D}_{\mathrm{NN}} \leq 1$ with values close to 0 for quark or gluon induced jets and close to 1 for hadronic tau decays. The distribution of the discriminant $\mathcal{D}_{NN}$ after the preselection is depicted in figure 3(b). The distributions of P_T^{miss} and $\Delta\phi_{\mathrm{miss}-\tau\mathrm{jet}}$ after requiring $\mathcal{D}_{NN} > 0.8$ are shown in figures 3(c),(d). This requirement yields a signal efficiency of 80% and a quark or gluon induced jet rejection of 95%. After all preselection criteria 16 (112) events are selected in $e^- p$ ($e^+ p$) data sample for $22.0 \pm 1.0 (stat.)$ $(121.1 \pm 5.3 (stat.))$ expected from the SM.

The final selection step in the hadronic tau decay channel makes use of the characteristic large missing transverse momentum carried by the tau neutrino which is expected to be in the direction of the tau-jet. The difference in ϕ between the missing transverse momentum vector and the tau-jet, $\Delta\phi_{\mathrm{miss}-\tau\mathrm{jet}}$, is required to be below $20°$. A minimal value of $P_T^{\mathrm{miss}} > 12\,\mathrm{GeV}$ is chosen for an accurate determination of the direction. In addition $P_T^{\mathrm{calo}} > 12\,\mathrm{GeV}$ is required. The final signal selection efficiency in the hadronic tau decay channel varies between 3% and 13%, normalised to all tau decays and limited by the branching fraction $BR(\tau^- \rightarrow \nu_\tau + \mathrm{hadrons}) = 64.8\%$ [28] (see table 2).

6 Systematic Uncertainties

The following experimental systematic uncertainties are considered:

- The energy of electrons is measured with a systematic uncertainty in the range from 0.7% to 3% depending on the polar angle. The uncertainty of the electron direction is estimated to be less than $3\,\mathrm{mrad}$ in θ and $1\,\mathrm{mrad}$ in ϕ.

- The scale uncertainty on the transverse momentum of high P_T muons amounts to 5%. The uncertainty on the reconstruction of the muon direction is $3\,\mathrm{mrad}$ in θ and $1\,\mathrm{mrad}$ in ϕ.

- For the hadronic final state, an energy scale uncertainty of 2% and a direction uncertainty of $20\,\mathrm{mrad}$ are assumed.

- The luminosity of the analysed datasets is known to 1.5%.

The effects of these systematic uncertainties on the signal and the expected SM background are evaluated by shifting the relevant quantities in the MC simulation by their uncertainty and adding all resulting variations in quadrature.

Systematic errors accounting for normalisation uncertainties on the expected background determined from the individual MC event generators are estimated to be 10% for NC DIS and Lepton-pair production, 15% for W production and 30% for photoproduction and CC DIS. The relatively large error of 30% on photoproduction and CC DIS is due to uncertainties on higher-order corrections. The errors associated to the background normalisation are added in quadrature to the experimental error to calculate the total error of the SM prediction.

The main theoretical uncertainty on the signal cross section originates from the parton densities. This uncertainty is estimated as described in [13]. It is found to be 5% for LQs coupling to up-type quarks and varies between 7% at low masses and 30% at masses around $290\,\mathrm{GeV}$ for LQs coupling to down-type quarks. The correlation between different channels is taken into account for the statistical interpretation and limit calculation [30]. A detailed description of the analysis can be found in [31].

7 Results

No candidate is found in the final data sample of the muon channel. The expected number of SM background events is 1.03 ± 0.32 in the e^+p set and 0.18 ± 0.06 in the e^-p sample. The largest contribution to this background comes from muon-pair production and the muonic decays of W bosons. These results apply equally to the muonic tau decay channel.

In the electronic tau decay channel no data event is found compared to a SM expectation of 0.28 ± 0.19 events in the e^-p sample and 1.24 ± 0.55 events in the e^+p data. NC DIS events with a mismeasured electron energy are the largest background contribution.

No e^-p data event passes the final selection criteria in the hadronic tau decay channel. The expected SM background amounts to 0.29 ± 0.06. One event is selected in the e^+p data for an expected SM prediction of 2.63 ± 0.57, dominated by NC DIS and photoproduction processes.

The results of the final selection in all channels are summarised in table 2. Typical signal selection efficiencies for some LQ types with a mass of $150\,\mathrm{GeV}$ and $500\,\mathrm{GeV}$ are also given. The observation is in agreement with the SM prediction and no evidence for LFV is found by the present analysis. Limits on the model parameters presented in section 3 are calculated as described in the following section.

8 Limits

The results of the search are interpreted in terms of exclusion limits on the mass and the coupling of LQs that may mediate LFV. The LQ production mechanism at HERA involves non-zero coupling to the first generation fermions $\lambda_{eq} > 0$. The LFC decays $\mathrm{LQ} \to eq$ or $\mathrm{LQ} \to \nu_e q$ are therefore possible. In order to cover the full LQ decay width and to generalise the results of LFV searches in ep collisions to an arbitrary weight between the LFC and LFV decay channels, the searches for LFC decays presented in [13] are combined with each of the LFV search channels μX or τX of the present analysis. It is assumed that only one of the couplings $\lambda_{\mu q}$ and $\lambda_{\tau q}$ is non–zero and therefore the μX and τX channels enter the limits calculation separately. A modified frequentist method with a likelihood ratio as the test statistic is used to combine the individual data sets and search channels [32].

In first generation LQ signals are searched for in about 400 bins in the $m_{\mathrm{LQ}} - y$ plane and the observed data is in agreement with the irreducible SM NC and CC background [13]. For the LFV channel μq (τq), the couplings λ_{eq} and $\lambda_{\mu q}$ ($\lambda_{\tau q}$) and the LQ mass determine the total production cross section, which is compared to the selected data from the LFV search channel and the first generation results. A combined test statistic is built and used to set limits as a function of λ_{eq}, $\lambda_{\mu q}(\lambda_{\tau q})$ and m_{LQ}. This procedure implicitly includes in the analysis the decays to a neutrino of any flavour and a quark.

Figure 4 shows limits before and after combination with the search for first generation LQs for the LQ types S_0^L and V_0^L up to LQ masses of $320\,\mathrm{GeV}$ assuming $\lambda_{eq} = \lambda_{\mu q}$ and $\lambda_{eq} = \lambda_{\tau q}$, i.e. $\beta_{\mathrm{LFV}} = 0.5$, in the resonance production region. The comparison for these types exemplifies that the limits on those LQs which can decay to a neutrino-quark pair, namely S_0^L, S_1^L, V_0^L and V_1^L, benefit most from the combination with the search for first generation LQs which covers decays to a neutrino-quark pair. In the high mass regime $m_{\mathrm{LQ}} \gg \sqrt{s}$ (contact interaction region) the obtained limits are similar to those deduced without the combination. The fluctuations in the combined limits are due to the observed data events in the search for first generation LQs. In the mass range from $250\,\mathrm{GeV}$ to $300\,\mathrm{GeV}$ both the combined limits on $\lambda_{\mu q}$ and $\lambda_{\tau q}$ are for all LQ types up to a factor 2 more stringent than without combination. Table 3 shows the 95% CL combined lower limits on the LQ mass for all LQ types assuming a coupling of electromagnetic strength $\lambda_{eq} = \lambda_{\mu q}(\lambda_{\tau q}) = 0.3$.

Allowing for an arbitrary decay rate between the LFC and LFV decay channels, β_{LFV}, the excluded regions for two LQ types and four mass values in the $\lambda_{\mu q_1} - \lambda_{eq_1}$ (a,b) and $\lambda_{\tau q_1} - \lambda_{eq_1}$ (c,d) planes are presented in figure 5. For very low values of β_{LFV} ($\lambda_{eq} \gg \lambda_{\mu q}(\lambda_{\tau q})$), the limits on λ_{eq} reproduce the bounds published in [13], as expected, since the LFC channel dominates the LQ width. For $\beta_{\mathrm{LFV}} \gg 0.5$ ($\lambda_{\mu q}(\lambda_{\tau q}) \gg \lambda_{eq}$) the present analysis extends significantly the published limits on λ_{eq} to lower values. The limit without combination in the contact interaction region (where the cross section is proportional to $\lambda_{eq_i} \lambda_{\mu(\tau)q_j}/m_{\mathrm{LQ}}^2$) forms a cross-diagonal straight line following different values of β_{LFV}. The combination in the contact interaction region, e.g. $m_{\mathrm{LQ}} = 350\,\mathrm{GeV}$, barely strengthens the limit as the virtual effects of the high mass LQ contact interaction at low values of $\sqrt{\hat{s}}$ are marginal compared to the irreducible NC and CC DIS background. Fluctuations of the data may even result in a less stringent combined limit.

Figures 6 and 7 display the 95% CL upper limits on the coupling $\lambda_{\mu q}$ and $\lambda_{\tau q}$ of all 14 LQ types to a muon-quark pair and a tau-quark pair, respectively, as a function of the LQ mass

leading to LFV in ep collisions, assuming $\lambda_{eq} = \lambda_{\mu q}(\lambda_{\tau q})$. The limit curves referring to the LQ types S_0^L and $\tilde{S}_{1/2}^L$ are identical to profiles of the corresponding excluded regions following the value $\beta_{\text{LFV}} = 0.5$ in figure 5. The limits are most stringent at low LQ masses with values $\mathcal{O}(10^{-3})$ around $m_{\text{LQ}} = 100$ GeV. Corresponding to the steeply falling parton density function for high values of x, the LQ production cross section decreases rapidly and exclusion limits are less stringent towards higher LQ masses. For LQ mass values near the kinematical limit of 319 GeV, the limit corresponding to a resonantly produced LQ turns smoothly into a limit on the virtual effects of both an off-shell s-channel LQ process and a u-channel LQ exchange. At masses $m_{\text{LQ}} > \sqrt{s}$ the two processes contract to an effective four-fermion interaction, where the cross section is proportional to $(\lambda_{\mu(\tau)q}\lambda_{eq}/m_{\text{LQ}}^2)^2$. This feature is visible in the constant increase of the exclusion limit for masses above the ep centre-of-mass energy of $\sqrt{s} = 319$ GeV. Due to initial state QED radiation and very low parton densities for masses near $\sqrt{s}$ the "kink" of the transition region is shifted to somewhat smaller masses of around $290 - 300$ GeV.

It is noticeable that the limits on vector LQs are more stringent compared to those on the scalars, due to the considerably higher cross section and the slightly higher acceptance. In each plot those LQ types that have couplings to both u and d quarks exhibit the best limit. The limits corresponding to LQs coupling to a u quark are more stringent than those corresponding to LQs coupling to the d quark only, as expected from the larger u quark density in the proton. The LQs S_0^L and S_0^R (V_0^L and V_0^R) differ only by the decay into a neutrino and a quark of the lefthanded LQ. As this decay channel is not covered in the LFV decay channels, the left-handed LQ cannot be as strictly excluded as the right-handed one. This argument applies to the resonant production where the analysis is only sensitive to the partial width of the LQ. In the high mass region the limits for S_0^L and S_0^R (V_0^L and V_0^R) are similar, as the four-fermion interaction is independent of the decay width.

The limits on $\lambda_{\mu(\tau)q} = \lambda_{eq}$ derived from the virtual effects of a 500 GeV LQ are transformed into a limit on the value $\lambda_{\mu(\tau)q_j}\lambda_{eq_i}/m_{\text{LQ}}^2$ and shown in tables 4 and 5 for $F = 0$ LQs and in tables 6 and 7 for $F = 2$ LQs. For each LQ type the limit is calculated for the hypothesis of a process with only the quarks of flavours i and j involved. With respect to quark flavours, the selection criteria described in sections 4 and 5 are inclusive since no flavour tagging of the hadronic jet is used.

These results may be compared with constraints from low energy experiments, based on the non-observation of LFV in muon scattering and rare decays of mesons and leptons [28]. The interpretation in terms of leptoquark exchange and limits on $\lambda_{\mu(\tau)q_j}\lambda_{eq_i}/m_{\text{LQ}}^2$ [33] are also shown in tables 4, 5, 6 and 7. Bounds of similar magnitude are observed for processes involving $e \to \tau$ transitions and charm or bottom quarks. In these cases the limits obtained in the present analysis are often superior to those from low energy experiments.

The results on LFV in LQ production are directly comparable with those from the ZEUS experiment [34]. Similar limits are obtained. At hadron colliders LQs are mainly produced in pairs independently of the coupling, and therefore searches cannot constrain LFV couplings. Lower mass limits on the second and third generation leptoquarks extend up to 250 GeV and 150 GeV, respectively, depending on the type and the assumed decay branching ratios [35]. Similarly, second and third generation leptoquarks are pair produced in e^+e^- annihilation where typical lower mass bounds reach values of 100 GeV [36].

9 Conclusion

A search for lepton flavour violation processes induced by leptoquarks in ep collisions at a centre-of-mass energy of $319\,\mathrm{GeV}$ with the H1 experiment at HERA is presented. No signal for the LFV processes $ep \to \mu X$ or $ep \to \tau X$ is found. Constraints on LFV LQ couplings are set combining the LFV search with the search for first generation LQs. The limits are a factor of 2 to 4 more stringent and extend beyond the domain in LQ mass excluded by previous searches performed by the H1 experiment [7]. Exclusion limits on several scenarios of LFV transitions of the kind $eq_i \to \tau q_j$ are more stringent than limits from searches for certain rare meson or tau decays. Assuming a coupling of electromagnetic strength, leptoquarks mediating lepton flavour violating processes $e \to \mu$ and $e \to \tau$ can be ruled out up to masses of $459\,\mathrm{GeV}$ and $379\,\mathrm{GeV}$, respectively.

Acknowledgements

References

[1] Y. Fukuda *et al.* [Super-Kamiokande Collaboration], Phys. Rev. Lett. **81** (1998) 1562 [hep-ex/9807003].

[2] Q. R. Ahmad *et al.* [SNO Collaboration], Phys. Rev. Lett. **89** (2002) 011301 [nucl-ex/0204008].

[3] J. C. Pati and A. Salam, Phys. Rev. D **81** (1974) 275;
H. Georgi and S. L. Glashow, Phys. Rev. Lett. **32** (1974) 438;
P. Langacker, Phys. Rep. **72** (1981) 185.

[4] H. P. Nilles, Phys. Rep. **110** (1984) 1;
H. E. Haber and G. L. Kane, Phys. Rep. **117** (1985) 75.

[5] B. Schrempp and F. Schrempp, Phys. Lett. B **153** (1985) 101;
J. Wudka, Phys. Lett. B **167** (1986) 337.

[6] S. Dimopoulos and L. Susskind, Nucl. Phys. B **155** (1979) 237;
S. Dimopoulos, Nucl. Phys. B **168** (1980) 69;
E. Farhi and L. Susskind, Phys. Rev. D **20** (1979) 3404;
E. Farhi and L. Susskind, Phys. Rep. **74** (1981) 277.

[7] C. Adloff *et al.* [H1 Collaboration], Eur. Phys. J. C **11** (1999) 447 [Erratum-ibid. C **14** (2000) 553] [hep-ex/9907002].

[8] I. Abt *et al.* [H1 Collaboration], Nucl. Instrum. Meth. A **386** (1997) 310; I. Abt *et al.* [H1 Collaboration], Nucl. Instrum. Meth. A **386** (1997) 348.

[9] D. Pitzl *et al.*, Nucl. Instrum. Meth. A **454** (2000) 334 [arXiv:hep-ex/0002044].

[10] B. Andrieu *et al.* [H1 Calorimeter Group], Nucl. Instr. and Meth. A **336** (1993) 499; B. Andrieu *et al.* [H1 Calorimeter Group], Nucl. Instr. and Meth. A **350** (1994) 57.

[11] J. M. Butterworth, J. P. Couchman, B. E. Cox and B. M. Waugh, Comput. Phys. Commun. **153** (2003) 85 [hep-ph/0210022].

[12] W. Buchmüller, R. Rückl and D. Wyler, Phys. Lett. B **191** (1987) 442.

[13] A. Aktas *et al.* [H1 Collaboration], Phys. Lett. B **629** (2005) 9 [hep-ex/0506044].

[14] K. Rosenbauer, dissertation RWTH Aachen (in German), PITHA 95/16, July 1995.

[15] J. Pumplin *et al.* [CTEQ Collaboration], JHEP **0207** (2002) 012 [hep-ph/0201195].

[16] S. Bentvelsen, J. Engelen and P. Kooijman, Proc. of the Workshop "Physics at HERA" (1991), Eds. W. Buchmüller and G. Ingelman, Vol. 1, p. 23.

[17] H. Jung, Comput. Phys. Commun. **86** (1995) 147.

[18] T. Sjöstrand, Comput. Phys. Commun. **39** (1986) 347.

[19] G. A. Schuler and H. Spiesberger, Proc. of the Workshop "Physics at HERA" (1991), Eds. W. Buchmüller and G. Ingelman, Vol. 3, p. 1419.

[20] T. Sjöstrand, Comp. Phys. Comm. **82** (1994) 74.

[21] M. Glück *et al.*, Phys. Rev. D **46** (1992) 1973.

[22] A. Aktas *et al.* [H1 Collaboration], Phys. Lett. B **639** (2006) 21 [hep-ex/0603014].

[23] T. Abe, Comput. Phys. Commun. **136** (2001) 126 [hep-ph/0012029].

[24] U. Baur, J. A .M. Vermaseren and D. Zeppenfeld, Nucl. Phys. B **375** (1992) 3.

[25] R. Brun *et al.*, CERN-DD/EE-84-1 (1987).

[26] C. Adloff *et al.* [H1 Collaboration], Eur. Phys. J. C **19** (2001) 269 [hep-ex/0012052].

[27] C. Adloff *et al.* [H1 Collaboration], Eur. Phys. J. C **11** (1999) 447 [Erratum-ibid. C **14** (1999) 553] [hep-ex/9907002].

[28] S. Eidelman *et al.* [Particle Data Group], Phys. Lett. B **592** (2004) 1.

[29] A. Aktas *et al.* [H1 Collaboration], Eur. Phys. J. C **48** (2006) 699 [hep-ex/0604022].

[30] M. Botje, Eur. Phys. J. C **14** (2000) 285 [hep-ph/9912439].

[31] L. Lindfeld, "Search for Lepton Flavour Violation with the H1 Experiment at HERA", Ph.D. Thesis, University of Zurich, 2006, available at http://www-h1.desy.de/publications/theses_list.html.

[32] R. Barate *et al.* [LEP Working Group for Higgs boson searches], Phys. Lett. B **565** (2003) 61 [hep-ex/0306033].

[33] S. Davidson, D. C. Bailey and B. A. Campbell, Z. Phys. C **61** (1994) 613 [hep-ph/9309310];
E. Gabrielli, Phys. Rev. D **62** (2000) 055009 [hep-ph/9911539].

[34] S. Chekanov *et al.* [ZEUS Collaboration], Eur. Phys. J. C **44** (2004) 463 [hep-ex/0501070].

[35] V. M. Abazov *et al.* [D0 Collaboration], Phys. Lett. B **636** (2006) 183 [hep-ex/0601047];
B. Abbott *et al.* [D0 Collaboration], Phys. Rev. Lett. **81** (1998) 38 [hep-ex/9803009];
A. Abulencia *et al.* [CDF Collaboration], Phys. Rev. D **73** (2006) 051102 [hep-ex/0512055];
A. A. Affolder *et al.* [CDF Collaboration], Phys. Rev. Lett. **85** (2000) 2056 [hep-ex/0004003].

[36] G. Abbiendi *et al.* [OPAL Collaboration], Eur. Phys. J. C **31** (2003) 281 [hep-ex/0305053].

Type	J	F	Q	ep dominant process		Coupling	Branching ratio β_ℓ
S_0^L	0	2	$-1/3$	$e_L^- u_L \;\rightarrow$	$\begin{cases} \ell^- u \\ \nu_\ell d \end{cases}$	λ_L $-\lambda_L$	$1/2$ $1/2$
S_0^R	0	2	$-1/3$	$e_R^- u_R \;\rightarrow$	$\ell^- u$	λ_R	1
$\tilde{S}_0^R$	0	2	$-4/3$	$e_R^- d_R \;\rightarrow$	$\ell^- d$	λ_R	1
S_1^L	0	2	$-1/3$ $-4/3$	$e_L^- u_L \;\rightarrow$ $e_L^- d_L \;\rightarrow$	$\begin{cases} \ell^- u \\ \nu_\ell d \end{cases}$ $\ell^- d$	$-\lambda_L$ $-\lambda_L$ $-\sqrt{2}\lambda_L$	$1/2$ $1/2$ 1
$V_{1/2}^L$	1	2	$-4/3$	$e_L^- d_R \;\rightarrow$	$\ell^- d$	λ_L	1
$V_{1/2}^R$	1	2	$-1/3$ $-4/3$	$e_R^- u_L \;\rightarrow$ $e_R^- d_L \;\rightarrow$	$\ell^- u$ $\ell^- d$	λ_R λ_R	1 1
$\tilde{V}_{1/2}^L$	1	2	$-1/3$	$e_L^- u_R \;\rightarrow$	$\ell^- u$	λ_L	1
V_0^L	1	0	$+2/3$	$e_R^+ d_L \;\rightarrow$	$\begin{cases} \ell^+ d \\ \bar{\nu}_\ell u \end{cases}$	λ_L λ_L	$1/2$ $1/2$
V_0^R	1	0	$+2/3$	$e_L^+ d_R \;\rightarrow$	$\ell^+ d$	λ_R	1
$\tilde{V}_0^R$	1	0	$+5/3$	$e_L^+ u_R \;\rightarrow$	$\ell^+ u$	λ_R	1
V_1^L	1	0	$+2/3$ $+5/3$	$e_R^+ d_L \;\rightarrow$ $e_R^+ u_L \;\rightarrow$	$\begin{cases} \ell^+ d \\ \bar{\nu}_\ell u \end{cases}$ $\ell^+ u$	$-\lambda_L$ λ_L $\sqrt{2}\lambda_L$	$1/2$ $1/2$ 1
$S_{1/2}^L$	0	0	$+5/3$	$e_R^+ u_R \;\rightarrow$	$\ell^+ u$	λ_L	1
$S_{1/2}^R$	0	0	$+2/3$ $+5/3$	$e_L^+ d_L \;\rightarrow$ $e_L^+ u_L \;\rightarrow$	$\ell^+ d$ $\ell^+ u$	$-\lambda_R$ λ_R	1 1
$\tilde{S}_{1/2}^L$	0	0	$+2/3$	$e_R^+ d_R \;\rightarrow$	$\ell^+ d$	λ_L	1

Table 1: The 14 leptoquark (LQ) types of the Buchmüller-Rückl-Wyler classification [12] in the Aachen notation [14]. The LQ subscripts refer to the weak isospin and the superscripts refer to the lepton chirality. Columns 2-4 display the spin J, fermion number F and electrical charge Q. The dominant resonant production process in ep scattering and the corresponding coupling is shown in columns 5 and 6 respectively. Leptoquarks which couple to a left-handed lepton doublet and can decay into a neutrino-quark pair, have a charged lepton decay branching ratio of $\beta_\ell = \Gamma_{\ell q}/(\Gamma_{\ell q} + \Gamma_{\nu_\ell q}) = 1/2$.

H1	Search for LFV			e^-p : $13.7\,\mathrm{pb}^{-1}$		e^+p : $66.5\,\mathrm{pb}^{-1}$	
		Selection results		Selection efficiency			
Channel		Data	SM MC	m_{LQ}	S_0^R	$V_{1/2}^L$	V_0^R	$\tilde{S}_{1/2}^L$
$ep \to \mu X$	e^-p	0	0.18 ± 0.06	150 GeV	58.0%	60.9%	60.1%	57.7%
				500 GeV	47.2%	38.5%	42.3%	37.8%
	e^+p	0	1.03 ± 0.32	150 GeV	55.5%	57.9%	58.7%	55.8%
				500 GeV	40.9%	40.5%	36.6%	41.4%
$ep \to \tau X$	e^-p	0	0.75 ± 0.21	150 GeV	28.3%	27.6%	27.1%	28.1%
				500 GeV	21.3%	14.4%	17.1%	13.8%
	e^+p	1	4.90 ± 0.85	150 GeV	26.8%	26.4%	26.9%	27.0%
				500 GeV	17.0%	16.7%	14.1%	17.3%
$ep \to \tau X$ $\hookrightarrow \tau \to e\nu_e\nu_\tau$	e^-p	0	0.28 ± 0.19	150 GeV	9.0%	7.8%	7.6%	8.9%
				500 GeV	6.7%	4.0%	5.2%	3.8%
	e^+p	0	1.24 ± 0.55	150 GeV	8.3%	7.2%	7.3%	8.4%
				500 GeV	4.8%	5.1%	4.0%	5.3%
$ep \to \tau X$ $\hookrightarrow \tau \to \mu\nu_\mu\nu_\tau$	e^-p	0	0.18 ± 0.06	150 GeV	7.4%	7.6%	7.6%	7.4%
				500 GeV	6.3%	4.7%	5.4%	4.6%
	e^+p	0	1.03 ± 0.32	150 GeV	7.8%	8.0%	8.1%	7.8%
				500 GeV	5.2%	5.2%	4.5%	5.3%
$ep \to \tau X$ $\hookrightarrow \tau \to h\nu_\tau$	e^-p	0	0.29 ± 0.06	150 GeV	11.9%	12.2%	11.9%	11.8%
				500 GeV	8.3%	5.7%	6.5%	5.4%
	e^+p	1	2.63 ± 0.57	150 GeV	10.7%	11.2%	11.5%	10.8%
				500 GeV	7.0%	6.4%	5.6%	6.7%

Table 2: Summary of the selection results of the search for the LFV processes $ep \to \mu X$ and $ep \to \tau X$. The results of the individual tau decay channels are also shown. The errors on the SM MC expectation include statistical and systematic errors added in quadrature. Examples of signal selection efficiencies for leptoquarks of the types S_0^R, $V_{1/2}^L$, V_0^R and $S_{1/2}^L$ with masses m_{LQ} of 150 GeV and 500 GeV are also shown. For the tau decay channels the efficiencies are normalised to the sum of all tau decays.

H1	lower exclusion limits on m_{LQ} (GeV) at 95% CL						
$F = 0$	$S_{1/2}^{L}$	$S_{1/2}^{R}$	$\tilde{S}_{1/2}^{L}$	V_0^L	V_0^R	$\tilde{V}_0^R$	V_1^L
$eq \to \mu q$	302	309	288	299	298	333	459
$eq \to \tau q$	298	298	285	290	293	307	379
$F = 2$	S_0^L	S_0^R	$\tilde{S}_0^R$	S_1^L	$V_{1/2}^L$	$V_{1/2}^R$	$\tilde{V}_{1/2}^L$
$eq \to \mu q$	294	294	278	306	299	374	336
$eq \to \tau q$	293	294	276	295	282	302	297

Table 3: Lower exclusion limits at 95% CL on leptoquark masses m_{LQ} assuming $\lambda_{\mu q} = \lambda_{eq} = 0.3$ or $\lambda_{\tau q} = \lambda_{eq} = 0.3$.

$ep \to \mu X$	**H1**					$F = 0$
Upper exclusion limits on $\lambda_{eq_i}\lambda_{\mu q_j}/m_{\mathrm{LQ}}^2$ (TeV^{-2}) for lepton flavour violating leptoquarks at 95% CL						
$q_i q_j$	$S_{1/2}^L$ $e^-\bar{u}$ e^+u	$S_{1/2}^R$ $e^-(\bar{u}+\bar{d})$ $e^+(u+d)$	$\tilde{S}_{1/2}^L$ $e^-\bar{d}$ e^+d	V_0^L $e^-\bar{d}$ e^+d	V_0^R $e^-\bar{d}$ e^+d	$\tilde{V}_0^R$ $e^-\bar{u}$ e^+u	V_1^L $e^-(\sqrt{2}\bar{u}+\bar{d})$ $e^+(\sqrt{2}u+d)$
1 1	$\mu N \to eN$ 5.2×10^{-5} **1.4**	$\mu N \to eN$ 2.6×10^{-5} **1.1**	$\mu N \to eN$ 5.2×10^{-5} **2.0**	$\mu N \to eN$ 2.6×10^{-5} **1.3**	$\mu N \to eN$ 2.6×10^{-5} **1.3**	$\mu N \to eN$ 2.6×10^{-5} **0.9**	$\mu N \to eN$ 0.8×10^{-5} **0.4**
1 2	$D \to \mu\bar{e}$ 2.4 **1.4**	$K \to \mu\bar{e}$ 2×10^{-5} **1.2**	$K \to \mu\bar{e}$ 2×10^{-5} **2.0**	$K \to \mu\bar{e}$ 1×10^{-5} **1.5**	$K \to \mu\bar{e}$ 1×10^{-5} **1.5**	$D \to \mu\bar{e}$ 1.2 **1.1**	$K \to \mu\bar{e}$ 1×10^{-5} **0.5**
1 3	$*$	$B \to \mu\bar{e}$ 0.4 **2.1**	$B \to \mu\bar{e}$ 0.4 **2.1**	$B \to \mu\bar{e}$ 0.2 **1.6**	$B \to \mu\bar{e}$ 0.2 **1.6**	$*$	$B \to \mu\bar{e}$ 0.2 **1.6**
2 1	$D \to \mu\bar{e}$ 2.4 **4.2**	$K \to \mu\bar{e}$ 2×10^{-5} **2.9**	$K \to \mu\bar{e}$ 2×10^{-5} **4.1**	$K \to \mu\bar{e}$ 1×10^{-5} **1.7**	$K \to \mu\bar{e}$ 1×10^{-5} **1.7**	$D \to \mu\bar{e}$ 1.2 **1.5**	$K \to \mu\bar{e}$ 1×10^{-5} **0.7**
2 2	$\mu N \to eN$ 9.2×10^{-4} **6.0**	$\mu N \to eN$ 1.3×10^{-3} **3.7**	$\mu N \to eN$ 3×10^{-3} **4.8**	$\mu N \to eN$ 1.5×10^{-3} **2.5**	$\mu N \to eN$ 1.5×10^{-3} **2.5**	$\mu N \to eN$ 4.6×10^{-4} **3.1**	$\mu N \to eN$ 2.7×10^{-4} **1.3**
2 3	$*$	$B \to \bar{\mu}eK$ 0.3 **5.2**	$B \to \bar{\mu}eK$ 0.3 **5.2**	$B \to \bar{\mu}eK$ 0.15 **3.5**	$B \to \bar{\mu}eK$ 0.15 **3.5**	$*$	$B \to \bar{\mu}eK$ 0.15 **3.5**
3 1	$*$	$B \to \mu\bar{e}$ 0.4 **5.3**	$B \to \mu\bar{e}$ 0.4 **5.3**	V_{ub} 0.12 **1.8**	$B \to \mu\bar{e}$ 0.2 **1.8**	$*$	V_{ub} 0.12 **1.8**
3 2	$*$	$B \to \bar{\mu}eK$ 0.3 **7.0**	$B \to \bar{\mu}eK$ 0.3 **7.0**	$B \to \bar{\mu}eK$ 0.15 **2.8**	$B \to \bar{\mu}eK$ 0.15 **2.8**	$*$	$B \to \bar{\mu}eK$ 0.15 **2.8**
3 3	$*$	$\mu N \to eN$ 1.3×10^{-3} **8.3**	$\mu N \to eN$ 3×10^{-3} **8.3**	$\mu N \to eN$ 1.5×10^{-3} **4.3**	$\mu N \to eN$ 1.5×10^{-3} **4.3**	$*$	$\mu N \to eN$ 2.7×10^{-4} **4.3**

Table 4: Limits at 95% CL on $\lambda_{eq_i}\lambda_{\mu q_j}/m_{\mathrm{LQ}}^2$ for $F = 0$ leptoquarks (bold). Combinations of i and j shown in the first column denote the quark generation coupling to the electron and muon respectively. In each cell the first two rows show the process providing the most stringent limit from low energy experiments. The cases marked with '$*$' refer to scenarios involving a top quark, not considered in the present analysis. Highlighted H1 limits are more stringent than those from the corresponding low energy experiment.

$ep \rightarrow \tau X$	**H1**					$F = 0$
Upper exclusion limits on $\lambda_{eq_i}\lambda_{\tau q_j}/m_{\mathrm{LQ}}^2\,(\mathrm{TeV}^{-2})$ for lepton flavour violating leptoquarks at 95% CL						
q_iq_j	$S_{1/2}^L$ $e^-\bar{u}$ e^+u	$S_{1/2}^R$ $e^-(\bar{u}+\bar{d})$ $e^+(u+d)$	$\tilde{S}_{1/2}^L$ $e^-\bar{d}$ e^+d	V_0^L $e^-\bar{d}$ e^+d	V_0^R $e^-\bar{d}$ e^+d	$\tilde{V}_0^R$ $e^-\bar{u}$ e^+u	V_1^L $e^-(\sqrt{2}\bar{u}+\bar{d})$ $e^+(\sqrt{2}u+d)$
1 1	$\tau\to\pi e$ 0.4 **2.1**	$\tau\to\pi e$ 0.2 **1.8**	$\tau\to\pi e$ 0.4 **3.1**	$\tau\to\pi e$ 0.2 **2.1**	$\tau\to\pi e$ 0.2 **2.1**	$\tau\to\pi e$ 0.2 **1.5**	$\tau\to\pi e$ 0.06 **0.7**
1 2	**2.2**	$\tau\to Ke$ 6.3 **1.8**	$K\to\pi\nu\bar{\nu}$ 5.8×10^{-4} **3.2**	$\tau\to Ke$ 3.2 **2.5**	$\tau\to Ke$ 3.2 **2.5**	**1.7**	$K\to\pi\nu\bar{\nu}$ 1.5×10^{-4} **0.8**
1 3	*	$B\to\tau\bar{e}$ 0.3 **3.2**	$B\to\tau\bar{e}$ 0.3 **3.2**	$B\to\tau\bar{e}$ 0.13 **2.7**	$B\to\tau\bar{e}$ 0.13 **2.7**	*	$B\to\tau\bar{e}$ 0.13 **2.7**
2 1	**6.7**	$\tau\to Ke$ 6.3 **4.8**	$K\to\pi\nu\bar{\nu}$ 5.8×10^{-4} **6.9**	$\tau\to Ke$ 3.2 **2.8**	$\tau\to Ke$ 3.2 **2.9**	**2.3**	$K\to\pi\nu\bar{\nu}$ 1.5×10^{-4} **1.1**
2 2	$\tau\to 3e$ 5.0 **10.9**	$\tau\to 3e$ 8.0 **6.7**	$\tau\to 3e$ 17.0 **8.6**	$\tau\to 3e$ 9.0 **4.5**	$\tau\to 3e$ 9.0 **4.5**	$\tau\to 3e$ 3.0 **5.5**	$\tau\to 3e$ 1.6 **2.4**
2 3	*	$B\to\tau\bar{e}X$ 14.0 **9.3**	$B\to\tau\bar{e}X$ 14.0 **9.3**	$B\to\tau\bar{e}X$ 7.2 **6.3**	$B\to\tau\bar{e}X$ 7.2 **6.3**	*	$B\to\tau\bar{e}X$ 7.2 **6.3**
3 1	*	$B\to\tau\bar{e}$ 0.3 **9.1**	$B\to\tau\bar{e}$ 0.3 **9.1**	V_{ub} 0.12 **3.0**	$B\to\tau\bar{e}$ 0.13 **3.0**	*	V_{ub} 0.12 **3.0**
3 2	*	$B\to\tau\bar{e}X$ 14.0 **12.6**	$B\to\tau\bar{e}X$ 14.0 **12.6**	$B\to\tau\bar{e}X$ 7.2 **4.9**	$B\to\tau\bar{e}X$ 7.2 **4.9**	*	$B\to\tau\bar{e}X$ 7.2 **4.9**
3 3	*	$\tau\to 3e$ 8.0 **15.2**	$\tau\to 3e$ 17.0 **15.2**	$\tau\to 3e$ 9.0 **8.1**	$\tau\to 3e$ 9.0 **8.1**	*	$\tau\to 3e$ 1.6 **8.1**

Table 5: Limits at 95% CL on $\lambda_{eq_i}\lambda_{\tau q_j}/m_{\mathrm{LQ}}^2$ for $F = 0$ leptoquarks (bold). Combinations of i and j shown in the first column denote the quark generation coupling to the electron and tau respectively. In each cell the first two rows show the process providing the most stringent limit from low energy experiments. The cases marked with '$*$' refer to scenarios involving a top quark, not considered in the present analysis. Highlighted H1 limits are more stringent than those from the corresponding low energy experiment.

$ep \to \mu X$	**H1**					$F = 2$
Upper exclusion limits on $\lambda_{eq_i}\lambda_{\mu q_j}/m_{\mathrm{LQ}}^2$ (TeV^{-2})						
for lepton flavour violating leptoquarks at 95% CL						
$q_i q_j$	S_0^L $e^- u$ $e^+ \bar{u}$	S_0^R $e^- u$ $e^+ \bar{u}$	$\tilde{S}_0^R$ $e^-(u+d)$ $e^+(\bar{u}+\bar{d})$	S_1^L $e^-(u+\sqrt{2}d)$ $e^+(\bar{u}+\sqrt{2}\bar{d})$	$V_{1/2}^L$ $e^- d$ $e^+ \bar{d}$	$V_{1/2}^R$ $e^-(u+d)$ $e^+(\bar{u}+\bar{d})$	$\tilde{V}_{1/2}^L$ $e^- u$ $e^+ \bar{u}$
1 1	$\mu N \to eN$ 5.2×10^{-5} **2.0**	$\mu N \to eN$ 5.2×10^{-5} **2.0**	$\mu N \to eN$ 5.2×10^{-5} **2.6**	$\mu N \to eN$ 1.7×10^{-5} **1.0**	$\mu N \to eN$ 2.6×10^{-5} **1.1**	$\mu N \to eN$ 1.3×10^{-5} **0.6**	$\mu N \to eN$ 2.6×10^{-5} **0.8**
1 2	$K \to \pi\nu\bar{\nu}$ 1×10^{-3} **2.6**	$D \to \mu\bar{e}$ 2.4 **2.6**	$K \to \mu\bar{e}$ 2×10^{-5} **3.2**	$K \to \mu\bar{e}$ 1×10^{-5} **1.4**	$K \to \mu\bar{e}$ 1×10^{-5} **2.0**	$K \to \mu\bar{e}$ 1×10^{-5} **1.4**	$D \to \mu\bar{e}$ 1.2 **1.9**
1 3	$*$	$*$	$B \to \mu\bar{e}$ 0.4 **3.3**	V_{ub} 0.24 **1.6**	$B \to \mu\bar{e}$ 0.2 **2.5**	$B \to \mu\bar{e}$ 0.2 **2.5**	$*$
2 1	$K \to \pi\nu\bar{\nu}$ 1×10^{-3} **2.6**	$D \to \mu\bar{e}$ 2.4 **2.6**	$K \to \mu\bar{e}$ 2×10^{-5} **3.3**	$K \to \mu\bar{e}$ 1×10^{-5} **1.4**	$K \to \mu\bar{e}$ 1×10^{-5} **1.1**	$K \to \mu\bar{e}$ 1×10^{-5} **0.7**	$D \to \mu\bar{e}$ 1.2 **0.8**
2 2	$\mu N \to eN$ 9.2×10^{-4} **6.0**	$\mu N \to eN$ 9.2×10^{-3} **6.0**	$\mu N \to eN$ 3×10^{-3} **4.8**	$\mu N \to eN$ 2.5×10^{-3} **2.2**	$\mu N \to eN$ 1.5×10^{-3} **2.5**	$\mu N \to eN$ 6.7×10^{-4} **1.9**	$\mu N \to eN$ 4.6×10^{-4} **3.1**
2 3	$*$	$*$	$B \to \bar{\mu}eK$ 0.3 **5.2**	$B \to \bar{\mu}eK$ 0.15 **2.6**	$B \to \bar{\mu}eK$ 0.15 **3.5**	$B \to \bar{\mu}eK$ 0.15 **3.5**	$*$
3 1	$*$	$*$	$B \to \mu\bar{e}$ 0.4 **3.7**	$B \to \mu\bar{e}$ 0.4 **1.9**	$B \to \mu\bar{e}$ 0.2 **1.2**	$B \to \mu\bar{e}$ 0.2 **1.2**	$*$
3 2	$*$	$*$	$B \to \bar{\mu}eK$ 0.3 **7.0**	$B \to \bar{\mu}eK$ 0.15 **3.5**	$B \to \bar{\mu}eK$ 0.15 **2.8**	$B \to \bar{\mu}eK$ 0.15 **2.8**	$*$
3 3	$*$	$*$	$\mu N \to eN$ 3×10^{-3} **8.3**	$\mu N \to eN$ 2.5×10^{-3} **4.3**	$\mu N \to eN$ 1.5×10^{-3} **4.3**	$\mu N \to eN$ 6.7×10^{-4} **4.3**	$*$

Table 6: Limits at 95% CL on $\lambda_{eq_i}\lambda_{\mu q_j}/m_{\mathrm{LQ}}^2$ for $F = 2$ leptoquarks (bold). Combinations of i and j shown in the first column denote the quark generation coupling to the electron and muon respectively. In each cell the first two rows show the process providing the most stringent limit from low energy experiments. The cases marked with '$*$' refer to scenarios involving a top quark, not considered in the present analysis. Highlighted H1 limits are more stringent than those from the corresponding low energy experiment.

$ep \to \tau X$				**H1**			$F=2$
Upper exclusion limits on $\lambda_{eq_i}\lambda_{\tau q_j}/m_{\mathrm{LQ}}^2\ (\mathrm{TeV}^{-2})$ for lepton flavour violating leptoquarks at 95% CL							

q_iq_j	S_0^L e^-u $e^+\bar{u}$	S_0^R e^-u $e^+\bar{u}$	$\tilde{S}_0^R$ $e^-(u+d)$ $e^+(\bar{u}+\bar{d})$	S_1^L $e^-(u+\sqrt{2}d)$ $e^+(\bar{u}+\sqrt{2}\bar{d})$	$V_{1/2}^L$ e^-d $e^+\bar{d}$	$V_{1/2}^R$ $e^-(u+d)$ $e^+(\bar{u}+\bar{d})$	$\tilde{V}_{1/2}^L$ e^-u $e^+\bar{u}$
1 1	G_F 0.3 **3.0**	$\tau \to \pi e$ 0.4 **3.0**	$\tau \to \pi e$ 0.4 **4.2**	$\tau \to \pi e$ 0.1 **1.7**	$\tau \to \pi e$ 0.2 **1.8**	$\tau \to \pi e$ 0.1 **1.0**	$\tau \to \pi e$ 0.2 **1.2**
1 2	$K \to \pi\nu\bar{\nu}$ 5.8×10^{-4} **4.0**	**4.0**	$\tau \to Ke$ 6.3 **5.0**	$K \to \pi\nu\bar{\nu}$ 2.9×10^{-4} **2.1**	$K \to \pi\nu\bar{\nu}$ 2.9×10^{-4} **3.5**	$\tau \to Ke$ 3.2 **2.3**	**3.1**
1 3	$*$	$*$	$B \to \tau\bar{e}$ 0.3 **5.3**	V_{ub} 0.12 **2.7**	$B \to \tau\bar{e}$ 0.13 **4.2**	$B \to \tau\bar{e}$ 0.13 **4.2**	$*$
2 1	$K \to \pi\nu\bar{\nu}$ 5.8×10^{-4} **4.2**	**4.2**	$\tau \to Ke$ 6.3 **5.5**	$K \to \pi\nu\bar{\nu}$ 2.9×10^{-4} **2.3**	$K \to \pi\nu\bar{\nu}$ 2.9×10^{-4} **1.8**	$\tau \to Ke$ 3.2 **1.1**	**1.2**
2 2	$\tau \to 3e$ 5.0 **10.8**	$\tau \to 3e$ 5.0 **10.9**	$\tau \to 3e$ 17.0 **8.6**	$\tau \to 3e$ 14.0 **3.9**	$\tau \to 3e$ 9.0 **4.5**	$\tau \to 3e$ 4.0 **3.5**	$\tau \to 3e$ 3.0 **5.5**
2 3	$*$	$*$	$B \to \bar{\tau}eX$ 14.0 **9.3**	$B \to \bar{\tau}eX$ 7.2 **4.7**	$B \to \bar{\tau}eX$ 7.2 **6.3**	$B \to \bar{\tau}eX$ 7.2 **6.3**	$*$
3 1	$*$	$*$	$B \to \tau\bar{e}$ 0.3 **6.3**	$B \to \tau\bar{e}$ 0.13 **3.1**	$B \to \tau\bar{e}$ 0.13 **1.9**	$B \to \tau\bar{e}$ 0.13 **1.9**	$*$
3 2	$*$	$*$	$B \to \bar{\tau}eX$ 14.0 **12.6**	$B \to \bar{\tau}eX$ 7.2 **6.4**	$B \to \bar{\tau}eX$ 7.2 **4.9**	$B \to \bar{\tau}eX$ 7.2 **4.9**	$*$
3 3	$*$	$*$	$\tau \to 3e$ 17.0 **15.2**	$\tau \to 3e$ 14.0 **7.8**	$\tau \to 3e$ 9.0 **8.1**	$\tau \to 3e$ 4.0 **8.1**	$*$

Table 7: Limits at 95% CL on $\lambda_{eq_i}\lambda_{\tau q_j}/m_{\mathrm{LQ}}^2$ for $F=2$ leptoquarks (bold). Combinations of i and j shown in the first column denote the quark generation coupling to the electron and tau respectively. In each cell the first two rows show the process providing the most stringent limit from low energy experiments. The cases marked with '$*$' refer to scenarios involving a top quark, not considered in the present analysis. Highlighted H1 limits are more stringent than those from the corresponding low energy experiment.
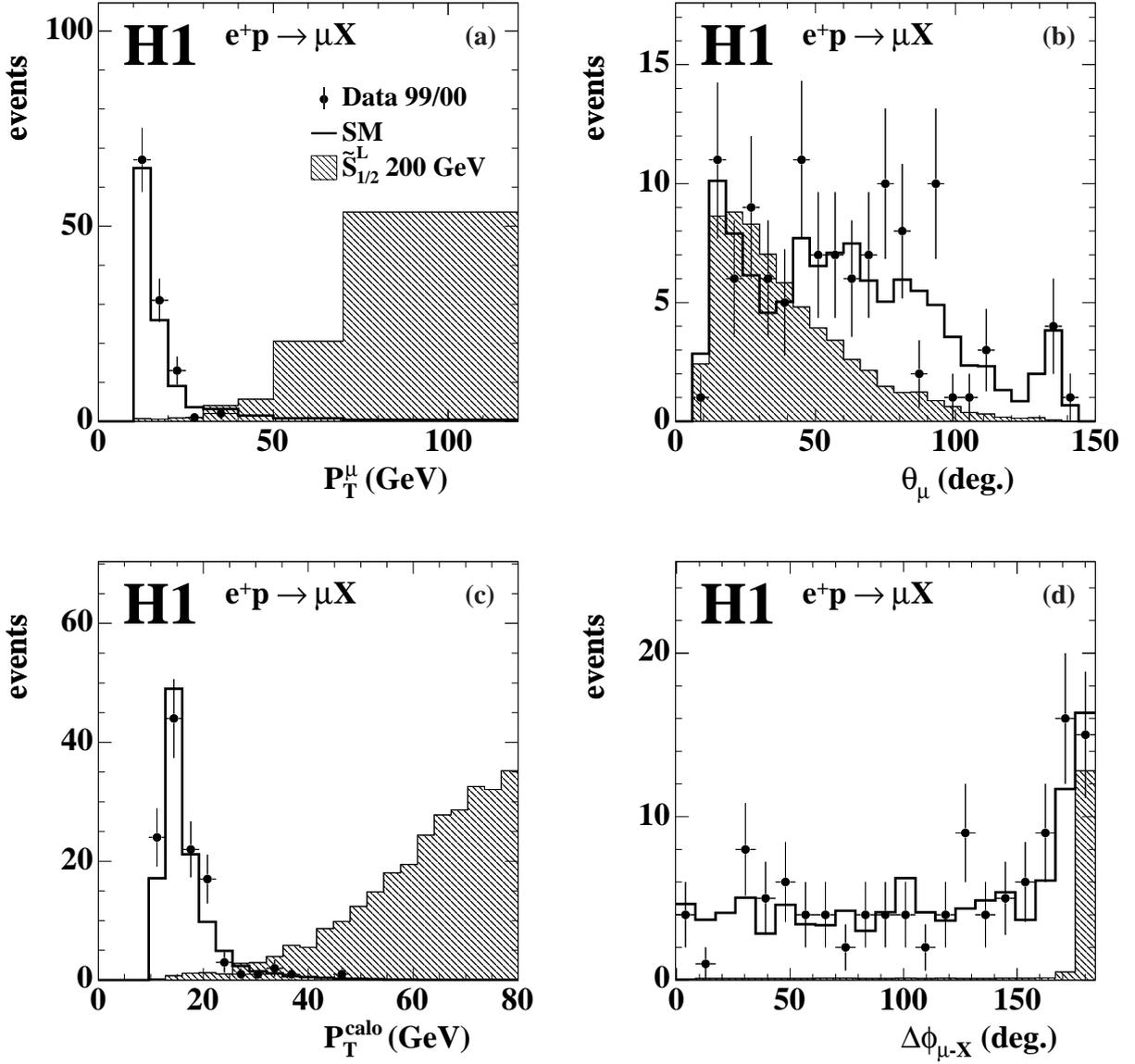
Figure 2: Control distributions of the preselected μX sample: (a) muon transverse momentum, (b) muon polar angle, (c) transverse momentum as measured from the calorimeter deposits and (d) acoplanarity between the muon and the hadronic final state X. Data (points) from e^+p collisions are compared to the SM expectation (histogram). The LFV signal MC sample of a leptoquark $\tilde{S}^L_{1/2}$ with $m_{\mathrm{LQ}} = 200\,\mathrm{GeV}$ and $\lambda_{eq} = \lambda_{\mu q} = 0.3$ is shown hatched with arbitrary normalisation in each plot.
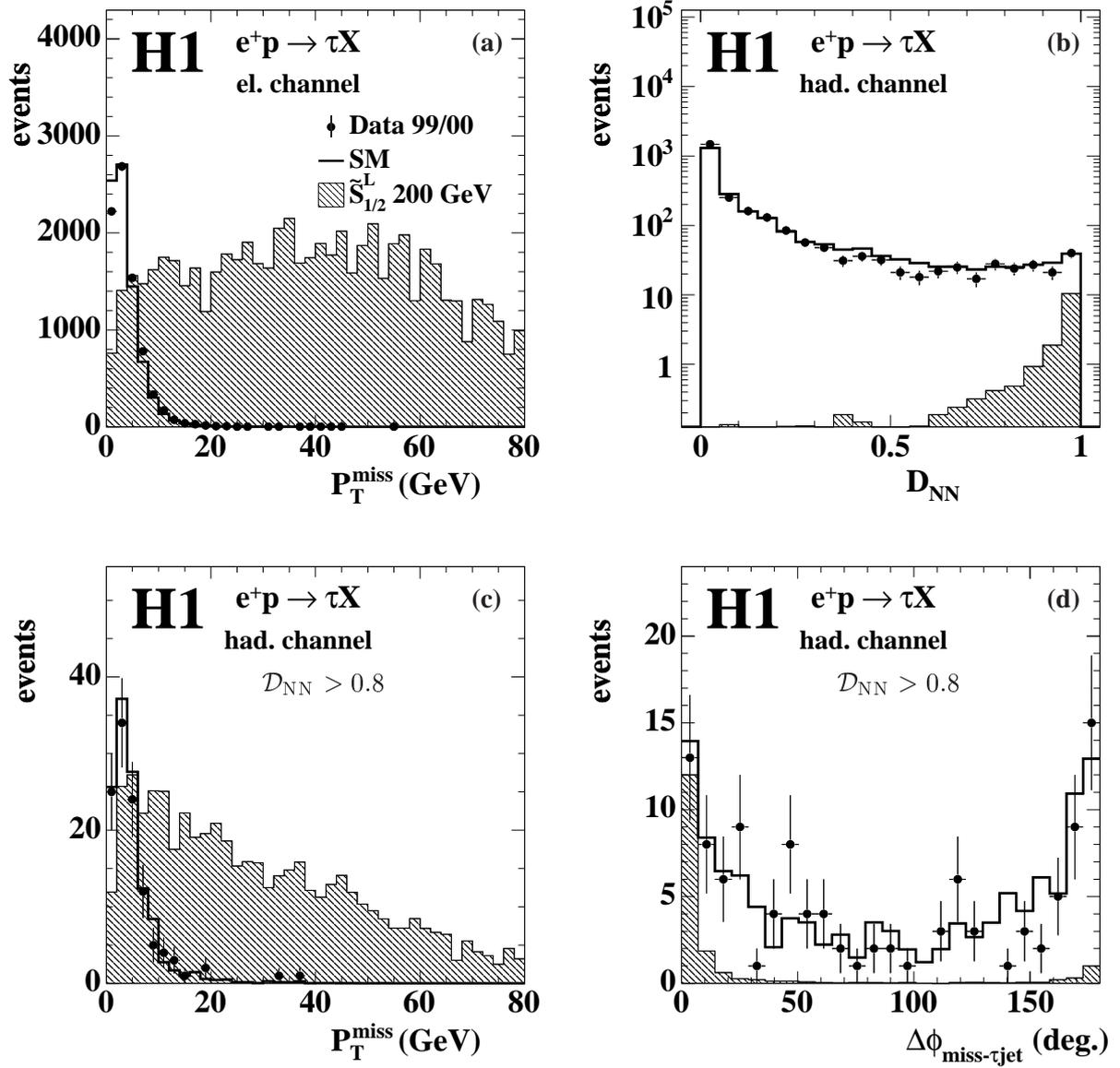
Figure 3: Distributions of the preselected τX sample: (a) missing transverse momentum in the electronic tau decay channel and (b) neural net tau-jet discriminant after the preselection in the hadronic tau decay channel. The restricted sample obtained after the additional cut $\mathcal{D}_{\mathrm{NN}} > 0.8$ in the hadronic channel: (c) missing transverse momentum and (d) acoplanarity between the tau-jet and the missing transverse momentum. The LFV signal MC sample of a leptoquark $\tilde{S}_{1/2}^{L}$ with $m_{\mathrm{LQ}} = 200\,\mathrm{GeV}$ and $\lambda_{eq} = \lambda_{\tau q} = 0.3$ is shown hatched with arbitrary normalisation in each plot.
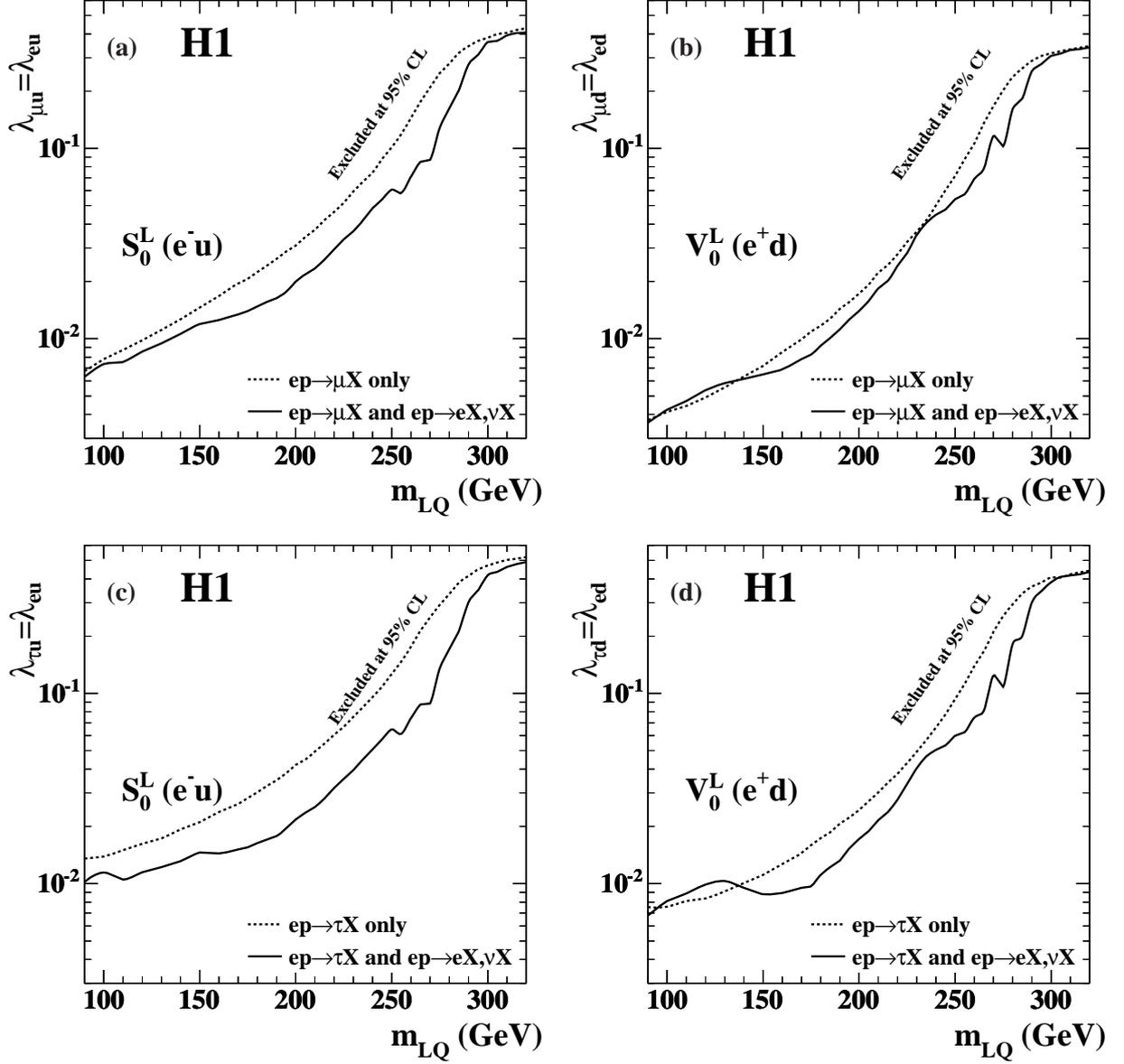
25

Figure 4: Comparison of limits at 95% CL on the coupling constants $\lambda_{\ell q}$ under the assumption $\lambda_{\ell q} = \lambda_{eq}$ as a function of the leptoquark mass m_{LQ} for: (a) S_0^L on $\lambda_{\mu u} = \lambda_{eu}$, (b) V_0^L on $\lambda_{\mu d} = \lambda_{ed}$, (c) S_0^L on $\lambda_{\tau u} = \lambda_{eu}$, and (d) V_0^L on $\lambda_{\tau d} = \lambda_{ed}$. The areas above the dashed lines represent the exclusion regions using only the lepton flavour violating leptoquark decay channels $ep \to \mu X$ and $ep \to \tau X$, respectively. The limits after combination with the results of the search for first generation leptoquarks are shown as solid lines.

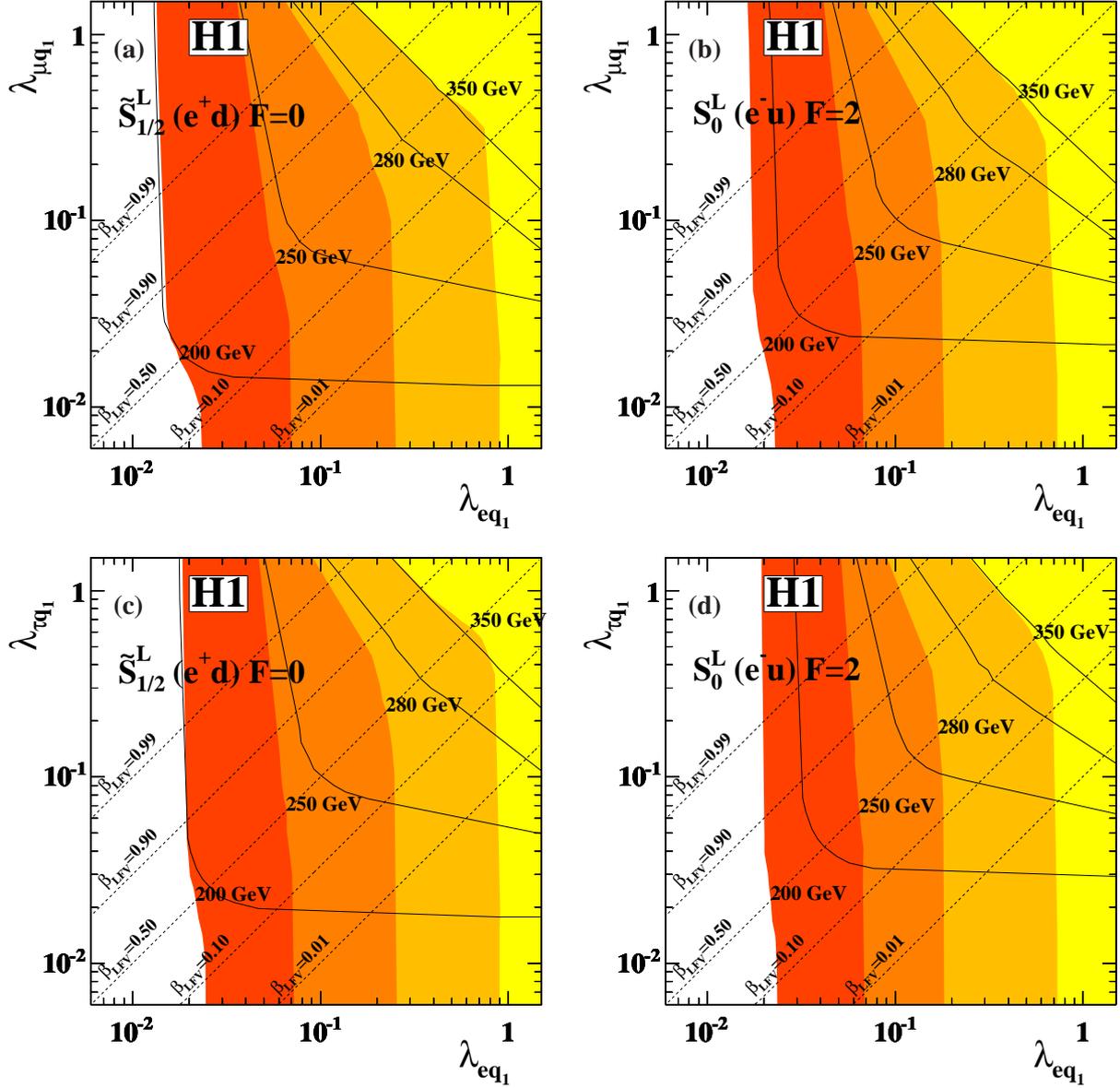## H1   Search for lepton flavour violation

Figure 5: Excluded regions at 95% CL (filled) on $\lambda_{\ell q_1}$ as a function of λ_{eq_1} for four different leptoquark masses. The branching ratio $\beta_{\mathrm{LFV}} = \lambda_{\ell q_1}^2/(\lambda_{\ell q_1}^2 + \lambda_{eq_1}^2)$ is not fixed. Diagonal dashed lines represent iso-curves for fixed values of β_{LFV}. The bounds deduced without the combination with first generation leptoquarks are shown as black curves corresponding to the different mass assumptions.

H1   Search for lepton flavour violation
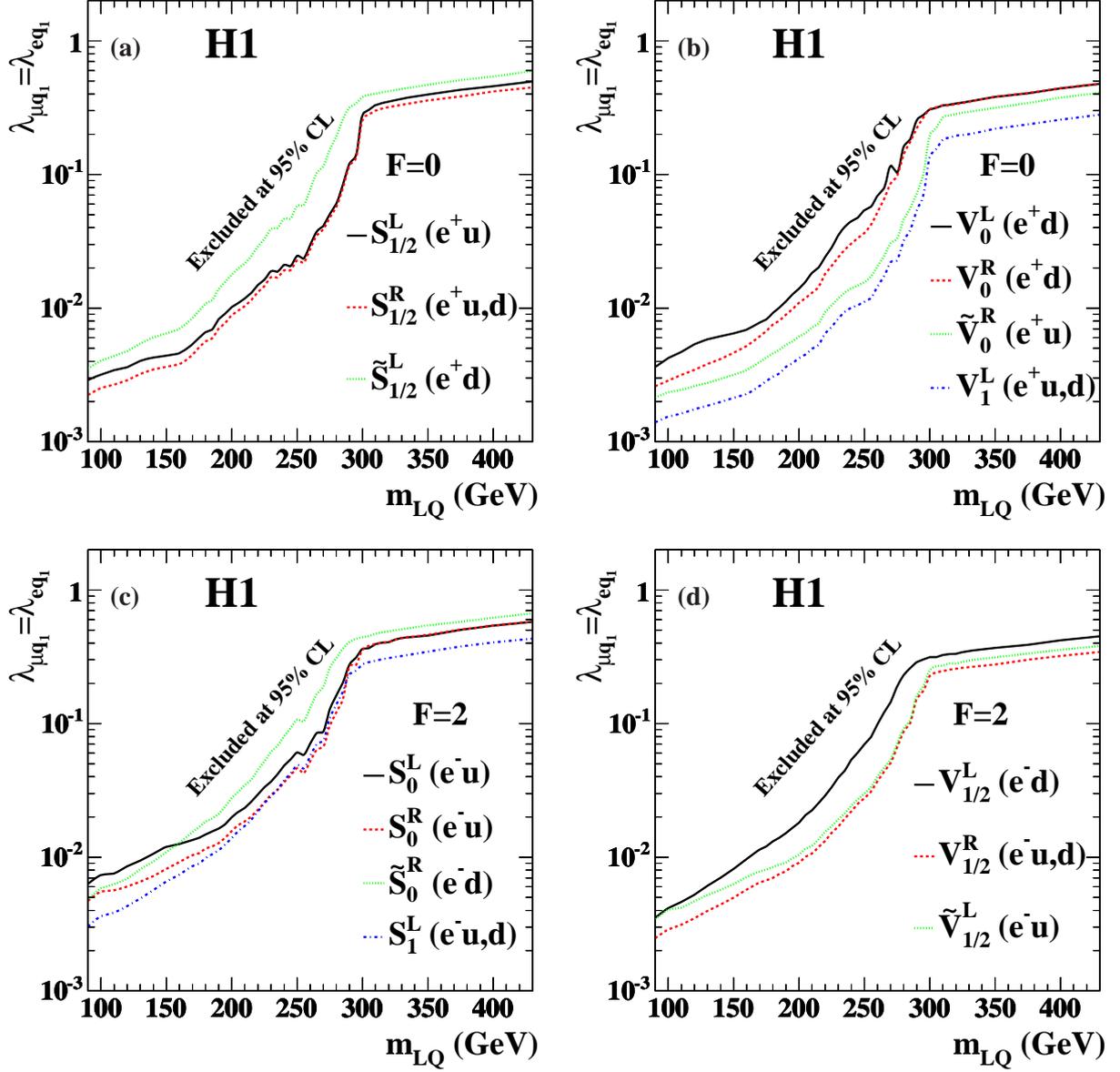
Figure 6: Limits on the coupling constants $\lambda_{\mu q_1} = \lambda_{e q_1}$ as a function of the leptoquark mass m_{LQ} for (a), (b) $F = 0$ and (c), (d) $F = 2$ scalar and vector leptoquarks. Regions above the lines are excluded at 95% CL. The notation q_1 illustrates that only processes involving first generation quarks are considered.
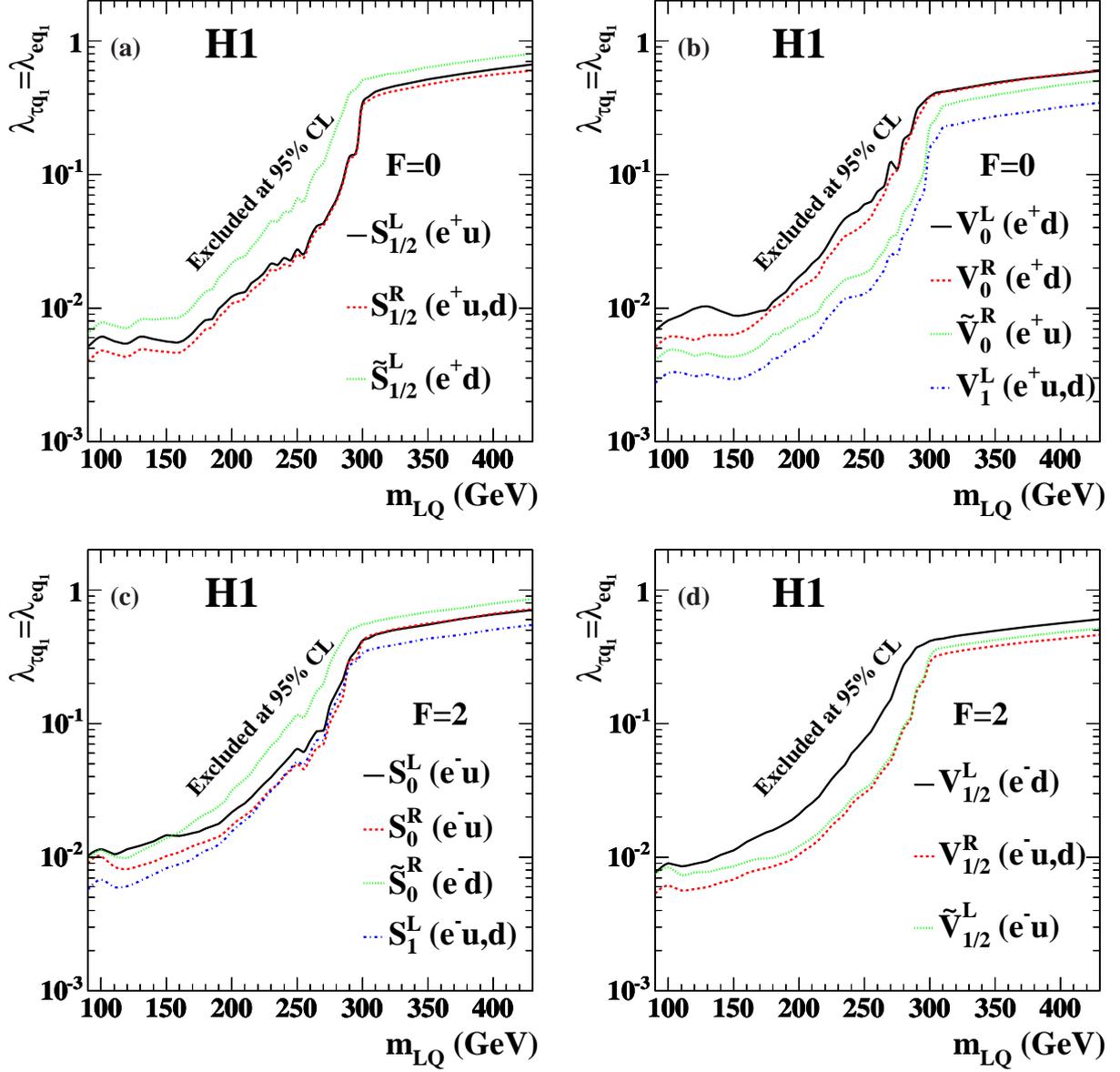
H1   Search for lepton flavour violation

Figure 7: Limits on the coupling constants $\lambda_{\tau q_1} = \lambda_{eq_1}$ as a function of the leptoquark mass m_{LQ} for (a), (b) $F = 0$ and (c), (d) $F = 2$ scalar and vector leptoquarks. Regions above the lines are excluded at 95% CL. The notation q_1 illustrates that only processes involving first generation quarks are considered.